Cell Reports

Article

Genomic context influences translesion synthesis DNA polymerase-dependent mechanisms of micronuclei induction by G-quadruplexes

Graphical abstract

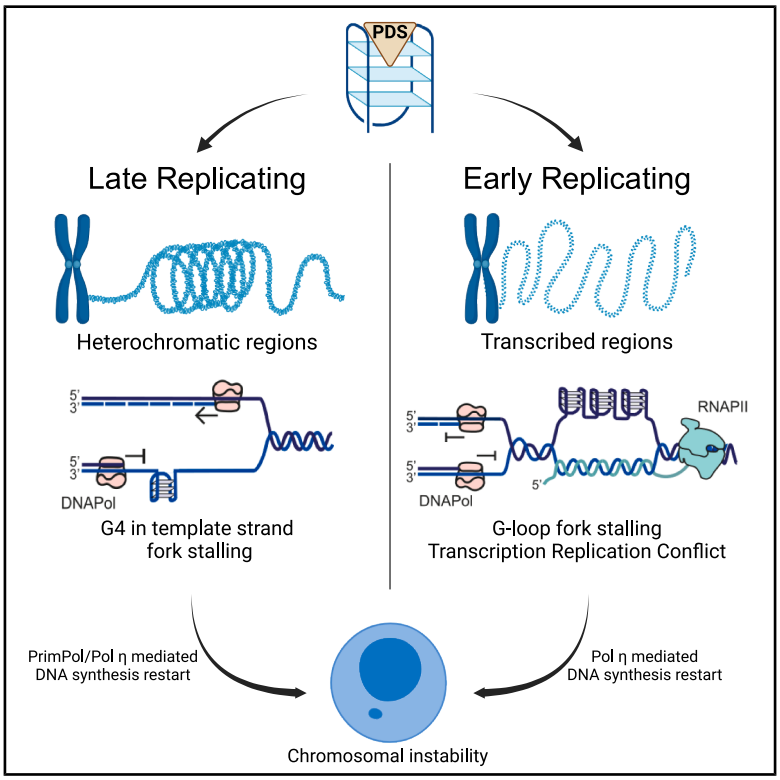

Highlights

- Genomic context influences fork stalling and restart after G4 stabilization
- Fork stalling in early S phase is driven by G-loops and high transcription levels
- Stalled forks avoid immediate DNA breakage via re-priming/bypass mechanisms
- Micronuclei formation depends on Pol η in S phase and PrimPol in late S phase

Authors

Simona Pepe, Federico Guerra, Marco Russo, Renée C. Duardo, Giovanni Capranico

Correspondence

giovanni.capranico@unibo.it

In brief

Pepe et al. demonstrate that G4 stabilization triggers cell-phase-specific replication fork stalling and restart mechanisms, relying on translesion DNA polymerases. While avoiding immediate DNA breakage, these mechanisms increase the risk of chromosomal instability in mitosis, highlighting crucial genomic stability processes and potential targets for therapies in cancer diseases.

Pepe et al., 2025, Cell Reports *44*, 115706
May 27, 2025
https://doi.org/10.1016/j.celrep.2025.115706

CellPress

Cell Reports

CellPress
OPEN ACCESS

Article

Genomic context influences translesion synthesis DNA polymerase-dependent mechanisms of micronuclei induction by G-quadruplexes

Simona Pepe,[1] Federico Guerra,[1] Marco Russo,[1,2] Renée C. Duardo,[1,3] and Giovanni Capranico[1,2,4,*]
[1]Department of Pharmacy and Biotechnology, University of Bologna, Bologna, Italy
[2]Preclinical & Translational Research in Oncology (PRO), IRCCS Azienda Ospedaliero-Universitaria di Bologna, Bologna, Italy
[3]Present address: IRCCS Azienda Ospedaliero-Universitaria di Bologna, Bologna, Italy
[4]Lead contact
*Correspondence: giovanni.capranico@unibo.it
https://doi.org/10.1016/j.celrep.2025.115706

SUMMARY

Guanine quadruplexes (G4s) are non-canonical DNA structures that can trigger micronuclei (MNi). Mechanisms of micronuclei formation by G4s are not fully understood. Here, we show that G4 stabilization can trigger cell-cycle-phase-specific mechanisms of replication fork stalling and DNA synthesis restart dependent on translesion synthesis (TLS) DNA polymerases (Pols). Fork stalling is caused by G-loops and high transcription during early S only. Moreover, while induction of micronuclei is dependent on DNA Pol η throughout S phase, primase and DNA-directed polymerase (PrimPol) is required in late S only. DNA breakage is not an immediate response to stabilized G4s but rather a consequence of persistent G4-mediated replication stress. Thus, different modes of fork stalling and restart, based on genomic context and TLS Pols, avoid immediate DNA breakage at stalled forks but at the expense of a risk of later mitotic chromosomal instability. The insights can lead to the development of more effective therapies for cancer and neurological diseases.

INTRODUCTION

Guanine quadruplexes (G4s) are nucleic acid secondary structures formed by stacked guanine base quartets, stabilized by Hoogsteen hydrogen bonds and K+ or Na+.[1–4] They are enriched at genome control sites, such as active gene promoters, telomeres, replication origins, and chromatin boundary elements, suggesting a role in genome function regulation.[5] G4s are dynamic structures, and their stability can be increased in living cells by specific G4 binders, such as Pyridostatin (PDS), CX-5461, and RHPS4, which showed potential for cancer therapy.[6,7] G4 stabilization can inhibit transcription and replication leading to genome instability in cancer cells, including micronuclei formation and mitotic errors.[1–3] Micronuclei are extra-nuclear organelles formed by chromatin portions surrounded by a nuclear membrane.[8] They arise from aberrant mitoses involving lagging chromosomes or chromatid fragments from sister chromatid non-disjunctions and anaphase bridges.[9–11] Micronuclei can be re-incorporated into the genome at the next mitosis leading to chromothripsis and increased chromosomal instability.[8,12] In addition, micronuclei chromatin can activate the cytoplasmic cGAS (2′,3′-cyclic GMP-AMP synthase)- stimulator of interferon response cGAMP interactor 1 (STING) pathway, triggering innate immune gene expression in cancer cells.[13–17] STING activation by micronuclei is actively investigated as a strategy to improve immunotherapy responses of cancer patients.[18,19]

The mechanism of micronuclei formation triggered by G4s is not fully understood as somewhat contrasting results have been reported. Genomic R-loops maps revealed that short PDS treatments induce both an increase and a spreading of pre-existing R-loops, particularly at highly transcribed genes, by forming G-loop structures.[3,20,21] R-loops are co-transcriptional nucleic acid structures formed by the annealing of nascent transcripts to the DNA strand template leading to RNA:DNA duplex hybrids and the non-transcribed strand being extruded as a single-stranded DNA loop.[22–24] Under various conditions, unbalanced R-loop levels can lead to DNA damage, replication fork stalling, transcription/replication conflicts (TRCs), and chromosomal instability.[2,23–26] Stalled replication forks can be restated by DNA cleavage-religation cycles mediated by MUS81 endo-nuclease and DNA ligase IV[27] coupled with G4 and R-loop resolution by specific helicases.[28,29] This mechanism can also involve primase and DNA-directed polymerase (PrimPol) activity, which mediates re-priming during replication restart at DNA lesions.[30] Consistently, micronuclei and DNA double-strand break (DSB) induction by G4 stabilization were shown to be mediated by R-loops.[20,28,29,31] In contrast, DNA replication restart from G4-induced stalled replication forks has been shown to occur without the need of DNA cuts and through a re-priming mechanism involving PrimPol, which can synthesize an RNA primer and then catalyze its extension with deoxyribonucleotide triphosphates (dNTPs).[32] PrimPol was proposed to promote restart of DNA synthesis downstream of a G4 obstacle in

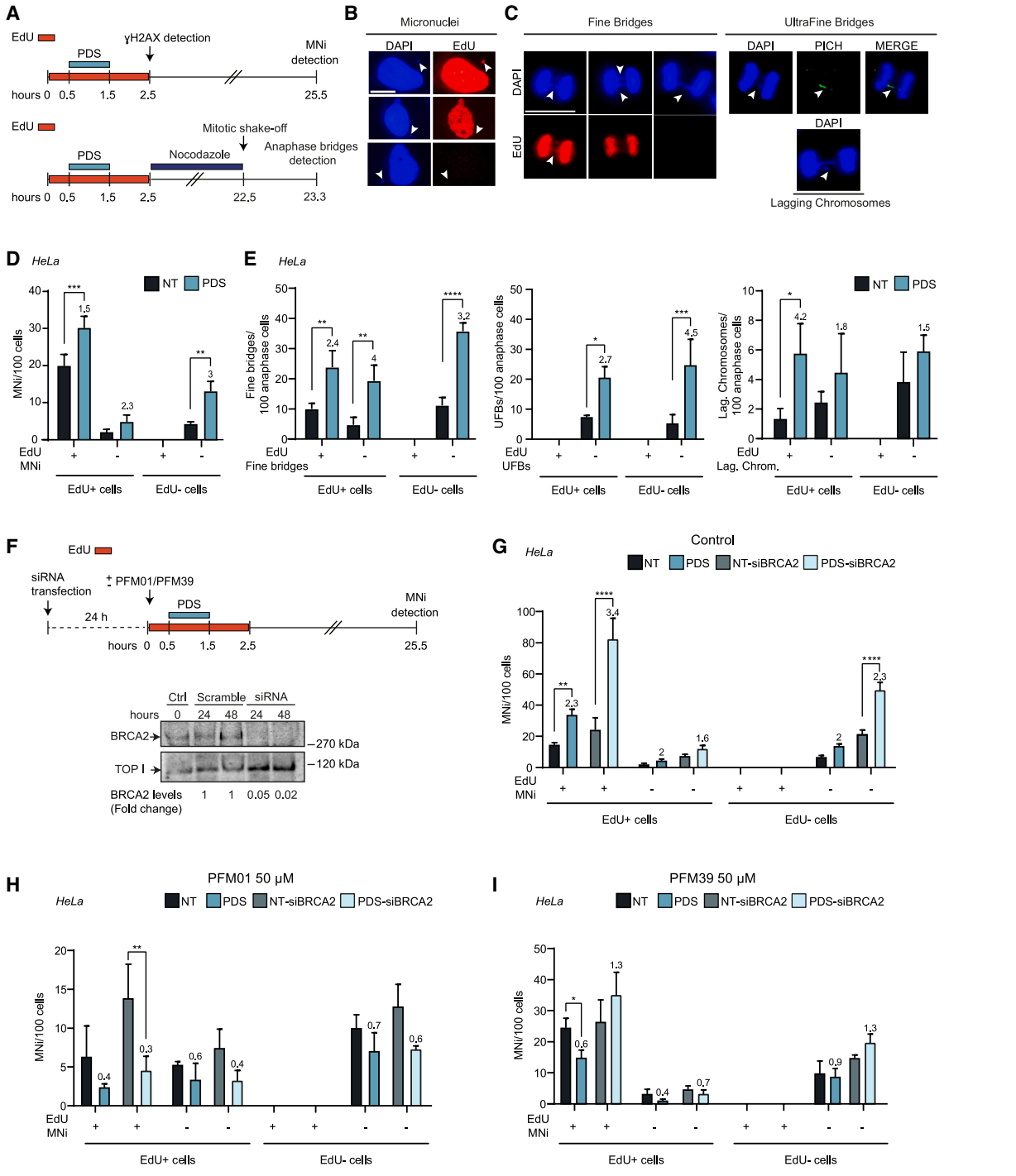

Figure 1. Stabilized G4s in S and no-S phases induce micronuclei and anaphase bridges, which are enhanced by Mre11 and prevented by BRCA2

(A) Experimental design for detecting micronuclei, γH2AX (top), and anaphase bridges (bottom).

(B) Representative images of EdU+/− cells and micronuclei (white arrows).

(C) DAPI-stained fine bridges and lagging chromosomes (Lag Chrom); ultrafine bridges (UFBs) detected with anti-PLK1-interacting checkpoint helicase (PICH) antibody.

(D) EdU+/EdU– MNi levels in EdU$^{+/-}$ HeLa cells. Bars show means ± SEM, n = 6. Average analyzed cells: 300.

(legend continued on next page)

the DNA template, allowing rapid resumption of replication and preventing fork collapse.[32] Moreover, recent studies with single-molecule imaging microscopy revealed that G4 spontaneously forms at strand templates of some active replication forks immediately behind mini chromosome maintenance (MCM) helicases, apparently without R-loop formation, and before nascent DNA synthesis.[33] Thus, published data leave undefined the precise mechanisms through which G4 stabilization leads to chromosomal instability.

In this work, we show that G4 stabilization by PDS can trigger cell-cycle phase-specific mechanisms of micronuclei formation dependent on the translesion synthesis (TLS) DNA polymerases, DNA polymerase η (Pol η), and PrimPol. In genomic regions replicating early or late during S phase, the mechanisms of fork stalling are different, involving G-loops and high transcription levels during early S only. The results also reveal that DNA breakage is not an immediate response to stabilized G4s, but rather a consequence of persistent G4-mediated replication stress. Thus, distinct modes of fork restart, based on genomic context and TLS Pols, avoid immediate DNA breakage likely maintaining a proper replication speed, but at the expense of a risk of later mitotic chromosomal instability. The understanding of genome instability mechanisms can lead to the development of effective therapeutic strategies for cancer and neurological diseases.

RESULTS

G4 stabilization can trigger chromosome instability during both S and no-S cell-cycle phases

Since stabilization of G4 structures is thought to induce replication stress eventually leading to micronuclei,[20,32] we first wondered whether G4 stabilization during S or no-S phases of the cell cycle leads to micronuclei formation at mitosis. We therefore determined micronuclei formation and mitotic errors in HeLa cells following 1-h treatment with 10 μM PDS, which effectively stabilizes nuclear G4s in living cells.[20] To distinguish cells in S phase at the time of PDS treatment, cells were labeled with 5-ethynyl-2′-deoxyuridine (EdU) and then cultured in drug- and label-free medium for 24 h before micronuclei detection by immunofluorescence microscopy (Figure 1A, upper panel). To determine mitotic errors, PDS-treated and EdU-labeled cells were grown in nocodazole-containing medium for 20 h followed by a mitotic shake-off (in Figure 1A, bottom panel). EdU labeling allowed to discriminate cells that were in S (EdU+) or no-S (EdU−) phases during PDS treatment.

PDS increased levels of micronuclei, anaphase fine and ultrafine bridges (UFBs), and lagging chromosomes during both S phase and no-S phases (Figures 1B–1E). The extent of micronuclei and anaphase bridges induction was even slightly higher for no-S than S cells (Figures 1D and 1E), suggesting that ongoing replication is not required at the time of G4 stabilization for chromosomal instability. Interestingly, PDS induced two different classes of micronuclei and anaphase bridges in EdU+ cells as some of them contained whereas others did not contain EdU-labeled DNA (EdU+ or EdU− micronuclei in Figures 1B–1E). Therefore, while many micronuclei and anaphase bridges contained chromatin fragments replicating at the time of G4 stabilization, a significant fraction of them contained only chromatin fragments, which were not replicated at the time of G4 stabilization. Assuming G4-induced micronuclei (and anaphase bridges) originated from chromatin suffering replication stress,[34] the results suggested that EdU− micronuclei chromatin can be either not fully replicated or replicated hours later after replication stress caused by G4 stabilization.

As breast cancer type 2 susceptibility protein (BRCA2) gene silencing increased PDS-induced micronuclei,[20] and BRCA2-meiotic recombination 11 homolog A protein (Mre11) interplay can affect stalled fork stability,[35–37] we investigated whether BRCA2/Mre11 functions can mediate G4-dependent micronuclei formation in cells not replicating at the time of PDS treatment (EdU−). BRCA2 silencing increased micronuclei induced by 1-h PDS treatments (Figures 1F and 1G), and chemical inhibition of both Mre11 exo- and endo-nuclease activities abolished the formation of all micronuclei classes in both *BRCA2*-proficient and *BRCA2*-deficient cells (Figures 1H and 1I). PFM01 and PFM39 effects were different, since the former and the latter reduced PDS stimulation of micronuclei below and close to control levels, respectively (Figures 1H and 1I). Since Mre11 inhibitors may slow the cell cycle, we measured EdU-labeled cell distribution and live cell-cycle progression (Figures S1A–S1C). PFM01 and PFM39 slightly affect the mitotic index but not the mitotic time (Figure S1C). PDS increases the mitotic index. Thus, even though the mitotic index was increased similarly, PDS effect on micronuclei formation was strongly reduced by Mre11 inhibitors in comparison to cells not treated with Mre11 inhibitors. Therefore, the data clearly showed that G4-dependent micronuclei stimulation in *BRCA2*-silenced cells is rescued by Mre11 inhibitors (Figures 1H and 1I). Interestingly, the effects of Mre11-BRCA2 were very similar in EdU+ and EdU− cells (Figures 1G–1I). Since Bloom helicase (BLM) is required during G2/M phase for a proper resolution of anaphase bridges,[9,38,39] we investigated BLM role by chemical inhibition in EdU−/+ cells (Figures S1D–S1G). BLM inhibition in G2/M phase prevented anaphase bridge resolution as shown by markedly reduced replication protein A (RPA)-coated UFBs (Figure S1F, upper panel) and increased PITCH-labeled bridges as reported by others.[38] However, it increased nucleoplasmic bridges and isolated

(E) Fine bridges, UFBs, and Lag. Chrom. increase in EdU-labeled cells. Graphs show mean ± SEM, $n = 3$. Average analyzed cells: 90.

(F) Experimental design of BRCA2-silenced HeLa cells tested with/without Mre11 inhibitors (PFM01 and PFM39) (top). Immunoblot of BRCA2 in HeLa cells treated with scrambled (Scramble) or BRCA2-specific siRNAs. Topoisomerase I (TOP I) as loading control. BRCA2 expression levels in silenced (24 and 48 h) vs. scrambled (Scr.) samples reported as fold change.

(G–I) Micronuclei increase in HeLa cells treated with scrambled or BRCA2-specific siRNAs (siBRCA2) for 24 h before and after PDS treatment (G). Micronuclei increase assessed with/without Mre11 endo-nuclease (PFM01) (H) or exo-nuclease (PFM39) (I) inhibitors. Bars show mean ± SEM, $n = 3$. Average analyzed cells: 230 (G), 160 (H), or 250 (I).

$^{*}p < 0.05$, $^{**}p < 0.01$, $^{***}p < 0.001$, $^{****}p < 0.0001$ (t test). Scale bar 10 μm. See also Figure S1.

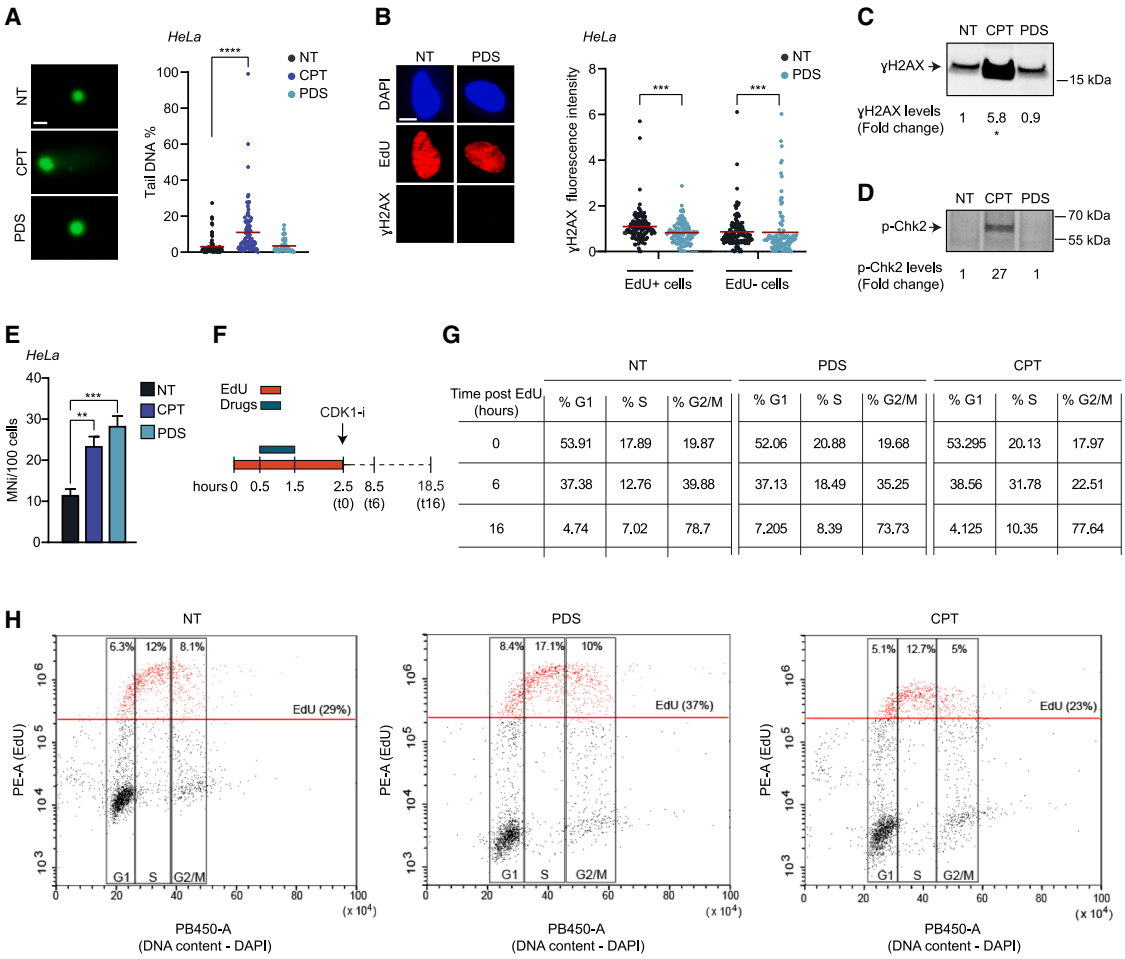

Time post EdU (hours)	NT % G1	NT % S	NT % G2/M	PDS % G1	PDS % S	PDS % G2/M	CPT % G1	CPT % S	CPT % G2/M
0	53.91	17.89	19.87	52.06	20.88	19.68	53.295	20.13	17.97
6	37.38	12.76	39.88	37.13	18.49	35.25	38.56	31.78	22.51
16	4.74	7.02	78.7	7.205	8.39	73.73	4.125	10.35	77.64

Figure 2. G4 stabilization does not induce immediate DNA damage

(A) DSB detection in HeLa cells after CPT/PDS treatment by neutral comet assay, $n = 2$. Average analyzed cells: 90. Representative images on the right.

(B) Representative images of DAPI-, EdU-, and anti-γH2AX-stained nuclei (left). γH2AX quantification after EdU administration (Figure 1A, top) (right). Bars show mean ± SEM, $n = 3$. Average analyzed cells: 200.

(C and D) Immunoblot of γH2AX (C) and pChk2 (D) in 1-h PDS/CPT-treated HeLa cells. Expression levels in treated vs. untreated samples reported as fold change, $n = 2$.

(E) Micronuclei quantitation in U2OS cells reported as MNi/100 cell. Average analyzed cells: 950. Graphs show mean ± SEM, $n = 3$.

(F) Experimental design for fluorescence-activated cell sorting (FACS) analysis of PDS/CPT-treated HeLa cells.

(G and H) FACS analysis of EdU-labeled HeLa cells treated with PDS/CPT. Table: percentage of G1, S, or G2/M phase cells at different times (0, 6, or 16 h) after EdU and CDK1-i (RO3306) administration (G). Graphs showing HeLa cell distribution in different cell-cycle phases after PDS/CPT treatment (t0 in F) (H) Percentage of total EdU+ cells (on the right "EdU [%]") and of EdU+ cells in G1, S, and G2/M-phase reported in each graph, $n = 2$.

*$p < 0.05$, **$p < 0.01$, ***$p < 0.001$, ****$p < 0.0001$ (two tailed Mann-Whitney test, A and B; t test, C–E). Scale bar 10 μm. See also Figure S2.

chromatin fragments resembling micronuclei in dividing EdU− cells (Figure S1G). Therefore, micronuclei and mitotic errors triggered by PDS-mediated G4 stabilization during no-S phases (G1 or G2/M) are dependent on the BRCA2/Mre11 interplay, known to affect stalled replication fork stability.[35–37]

DNA double-strand cleavage is not an immediate response to G4 stabilization by PDS

Since 24-h PDS treatments induced micronuclei in an R-loop-dependent manner,[20] we investigated the role of R-loops under our present conditions using human FLAG-tagged RNaseH1-expressing U2OS cells under an inducible promoter (Figure S2A). RNaseH1 expression markedly abrogated G4-induced micronuclei and anaphase bridges in both S and no-S phases (Figures S2B–S2E) highlighting R-loop role in chromosomal instability triggered in both phases. We next asked whether stabilized G4s induce DNA damage under the present conditions. Results clearly show that 1-h G4 stabilization did not increase DSBs as shown by neutral comet assay, S139-phosphorylated histone H2AX (γH2AX) foci, and cellular content (Figures 2A–2C and S2F) in either S or no-S phase cells. In agreement with previous results showing detectable DSB levels after at least 4 h of continuous G4 stabilization,[14,20] these results confirm that stabilized G4s do not trigger immediate DSBs in human cancer cells but cause DSBs only upon persistent G4 stabilization and replication stress.

These findings are in contrast with high levels of DSBs induced by similar brief treatments with camptothecin (CPT),[40] a DNA topoisomerase I poison (Figures 2A, 2C, 2D, S2F, and S2G), despite both drugs inducing comparable levels of micronuclei (Figure 2E). Moreover, PDS-treated cells showed a slight alteration of cell-cycle distribution after 6 and 16 h from the addition of a CDK1 inhibitor to arrest cells at G2 phase, whereas camptothecin-treated cells showed a higher fraction of cells in S phase than untreated and PDS-treated cells at 6 h (Figures 2F–2H) with almost full recovery after 16 h (Figure 2G). Thus, 1-h exposure to camptothecin and PDS triggers similar micronucleus levels after 24 h; however, the two compounds markedly differ in DSB production and effects on S phase duration.

Overall, the data demonstrate that PDS-mediated G4 stabilization in S as well as no-S phases can lead to mitotic errors and micronuclei in a BRCA2/Mre11- and R-loop-dependent manner without DNA damage, though PDS slightly delays the cell cycle. Since a large fraction of no-S phase is constituted by G1 or G2 cells, G4 stabilization in these phases may cause replication stress upon cells entering S phase.

Micronuclei are induced by stabilized G-loops during early S phase only

The aforementioned results suggest that stabilized G4s induce molecular alterations that persist after PDS removal, affecting replication when EdU− cells enter S phase. To test whether PDS triggers micronuclei formation when G1/G2-phase cells are exposed to it, we performed a dual-pulse nascent DNA labeling protocol. Cells were sequentially labeled with EdU and bromodeoxyuridine (BrdU) for 2.5 h each, with PDS added for 1 h during EdU incorporation (Figure 3A, top). The dual-pulse labeling experimental scheme allowed to split cells into four classes based on the cell-cycle phase at the time of cell exposure to PDS: early/mid S (EdU+/BrdU+), late S (EdU+/BrdU−), late G1 (EdU−/BrdU+), and early G1/G2M (EdU−/BrdU−) (Figure 3A, bottom). The results showed that PDS triggered micronuclei (MNi) formation in all classes (Figures 3B and S3A),[40] showing in particular that G4 stabilization in late G1 phase can eventually affect replication upon S phase entry and chromosomal stability at mitosis. Unlike PDS, camptothecin does not induce micronuclei in late S,[40] suggesting that G4 stabilization activates a specific mechanism during late replication. Interestingly, RNaseH1 overexpression in HeLa cells completely abrogated micronuclei formation when PDS treatment occurred in early/mid S, late G1, and early G1/G2M phases, but not in late S phase (Figures 3B and S3A). Moreover, RNaseH1 overexpression reduced PDS-mediated fine bridge formation in early/mid S but not in late S (Figure S3B). Thus, mitotic errors and micronuclei triggered by PDS during late S are both RNaseH1 insensitive.

We then asked whether other G4 binders have similar effects. We tested RHPS4 and CX-5461[44,45], G4 binders unrelated to PDS, in U2OS cells with or without RNaseH1 overexpression (Figures S3C and S3D). Although RHPS4 and CX-5461 induced micronuclei at different levels, both triggered RNaseH1-sensitive micronuclei, but not in late S cell category, similarly to PDS (Figure S3C). Thus, the specific mechanism elicited by G4 stabilization during late replication is independent from R-loops. Since the fraction of EdU+/BrdU− cells was minor with respect to the total population, it did not significantly impact RNaseH1 effects on micronucleus levels as detected with single-labeling experiments (Figures S2B and S2C).

Since R-loop dependency of PDS-induced micronuclei is restricted to late G1/early-mid S phase, we wondered whether PDS-induced R-loops preferentially localize at early replicating initiation zones (IZs). We analyzed PDS-increased genomic DNA:RNA hybrids after 5 min of treatment of U2OS cells[20] and compared PDS-induced hybrids to replicating IZs in the same U2OS cell line.[41] The results showed that PDS-induced hybrids were strongly and specifically enriched at early replicating IZs (Figure S3E). Since PDS can increase R-loop levels by extending previously formed hybrids,[20] we then restricted the analyses to PDS-extended hybrids showing that they were again highly enriched specifically in early replicating IZs (Figure 3C). Interestingly, G4-induced R-loops were enriched in constitutive as well as oncogene-induced early replicating IZs[41] (Figure 3C). Thus, this region-specific enrichment of PDS-induced hybrids is consistent with RNaseH1-mediated reduction of PDS-induced micronuclei specifically in late G1 and early/mid S phases.

Since R-loops are co-transcriptional structures[22,23] and G4 stabilization can lead to TRCs,[27] we next explored transcription role in chromosomal instability induced by G4 stabilization at specific cell-cycle phases. First, we determined the transcriptional status of R-loop regions enriched in IZs with public data of RNA polymerase II (RNAPII) density (by chromatin immunoprecipitation sequencing [ChIP-seq]) and of nascent transcripts (by GRO-seq, global run-on followed by sequencing) in U2OS cells.[42,43] A comparison of early replicating IZs associated with PDS-increased R-loops with those not associated with R-loops showed that the former, but not the latter, exhibited high levels of chromatin-bound RNAPII and GRO-seq signals. Thus, the former are highly transcribed regions whereas the latter are transcribed at much lower levels (Figure 3D). Then, we determined transcription elongation role on micronuclei formation by using the transcription elongation inhibitor 5,6-dichloro-1-α-*d*-ribofuranosylbenzimidazole (DRB). We found that DRB suppressed G4-induced micronuclei in late G1 and early/mid S, but not in late S (Figure 4A), showing that transcription elongation contributes to replication stress leading to micronuclei formation in a phase-specific manner.

We have recently established that transcription elongation is a key aspect of TRCs caused by the Topoisomerase I poison, camptothecin.[40] In particular, transcription factor II S (TFIIS) attenuates camptothecin-induced micronuclei due to its ability to rescue RNAPII arrest.[40] Therefore, we wondered whether TFIIS can attenuate micronuclei induction by G4 stabilization specifically in certain cell-cycle phases. By expressing a dominant-negative D290A and E291A TFIIS mutant (TFIISm)[46] in HEK293T cells, we determined the effects of G4 stabilization on micronucleus levels with the dual-pulse labeling scheme (Figure 3A). The results show that TFIISm expression increased micronucleus levels by G4 stabilization in early/mid S, but not in late S (Figures 4B and S4A). In each graph of Figure 4B, we split micronuclei into separated groups based on EdU/BrdU labeling patterns to show that TFIISm mainly affects certain micronuclei but not others. Thus, TFIIS attenuates G4-induced micronuclei specifically during early S phase, and not in late S,

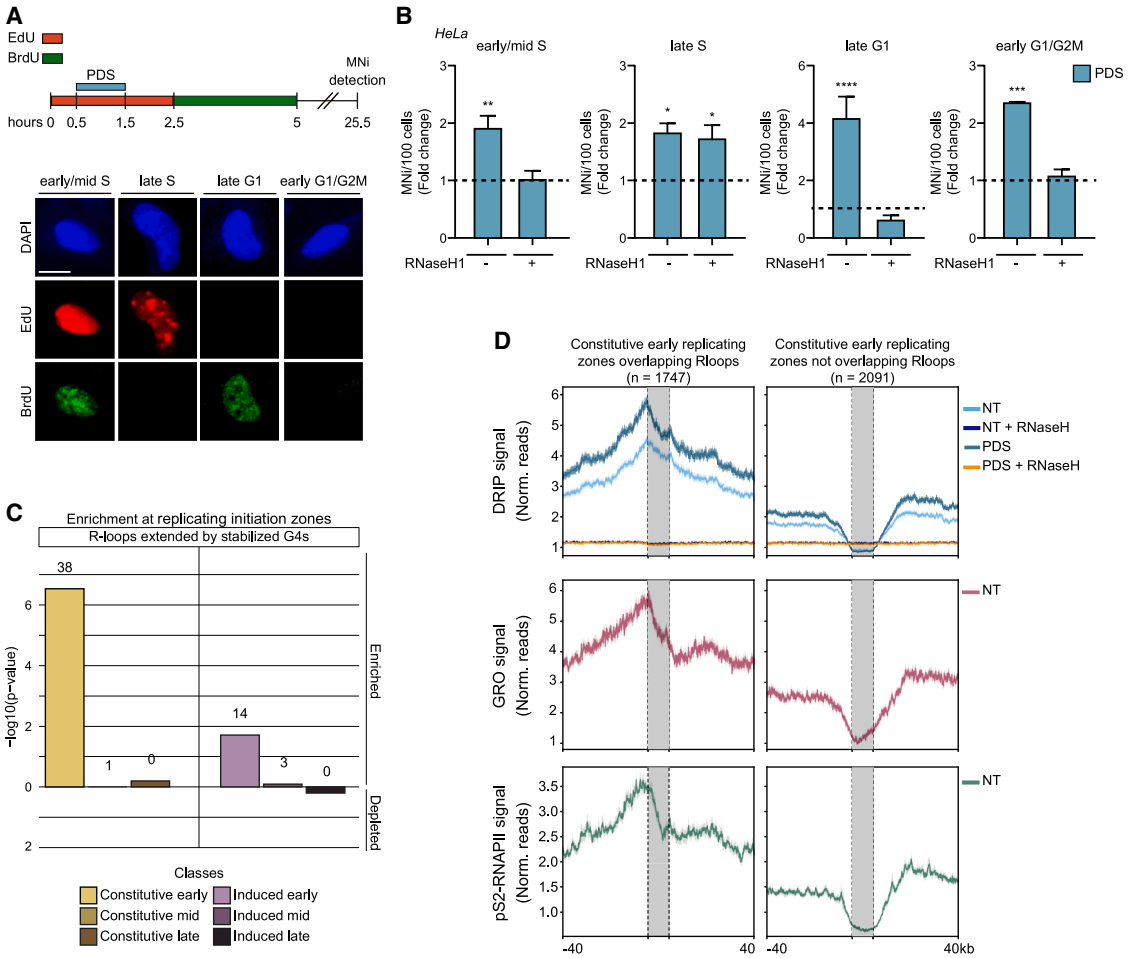

Figure 3. G4-induced R-loops are enriched at early replicating zones causing micronuclei exclusively in early/mid S and late G1 phases

(A) Experimental design for micronuclei detection in PDS-treated EdU-BrdU-labeled HeLa cells (top). Representative images of EdU-BrdU staining (bottom). Scale bar 10 μm

(B) Micronuclei quantitation in HeLa cells, transiently transfected with an RNAseH1-expressing plasmid, at early/mid S, late S, late G1, and early G1/G2M phases during PDS treatment. Micronuclei quantitation in PDS-treated vs. untreated samples is reported as fold change of MNi/100 cell. Dotted lines: control sample. Graphs show mean ± SEM, $n = 3$. Average analyzed cells: 250 (early/mid S), 100 (late S), 65 (late G1), and 500 (early G1/G2M). *$p < 0.05$, **$p < 0.01$, ***$p < 0.001$, ****$p < 0.0001$ (t test).

(C) Enrichment analysis of observed PDS-induced R-loops (R-loops extended by stabilized G4s) at constitutive or oncogene-induced (Induced) early, mid, and late replicating zones[41] vs. expected by randomization on gene regions $n = 100$. Barplots report binomial test p values (y axis) of enrichment. $-\log_{10}$ (p values) are referred to as "Enriched" or "Depleted" for enrichment or depletion over expected, respectively. The number of observed overlaps at each category is reported.

(D) Metaplot showing normalized mean levels (Norm. reads) of hybrids (DNA-RNA immunoprecipitation, DRIP),[20] nascent transcripts (GRO),[42] and phosphorylated-Ser2-RNA polymerase II (pS2-RNAPII)[43] at constitutive early replicating domains[41] overlapping an R-loop (left panels) or not (right panels). Gray-shaded area indicates constitutive regions of 10 kilobases (kb) in a window of +/− 40 kb. See also Figure S3.

supporting that G4 stabilization at highly transcribed, early replicating IZs induces hybrid-dependent TRCs leading to micronuclei formation at the following mitosis.

Next, we wondered whether G-loops affect replication forks in a phase-dependent manner. We then analyzed PDS-induced replication fork stalling in early and late S phases by DNA fiber assay in synchronized HeLa cells (Figures S4B and S4C). PDS induces an immediate slowdown of DNA synthesis, rescued by RNaseH1 overexpression and DRB treatment when 95% of cell population was in early S (Figures 4C, 4D, S4B, and S4C). In contrast, PDS-induced replication slowdown was only partially dependent, if any, on transcription and hybrids when 41% of cells were in late S and only 2% in early S (Figures 4C, 4D, S4B, and S4C). Thus, replication fork stalling in late S is largely independent of transcription and R-loop formation.

PrimPol is needed at late S phase to trigger micronuclei by PDS

Re-priming of DNA synthesis can bypass obstacles in the template strand at stalled replication forks.[2,25] Since PrimPol is the main enzyme responsible for re-priming at G4-stalled forks,[32] we investigated its phase-specific effects on PDS-induced

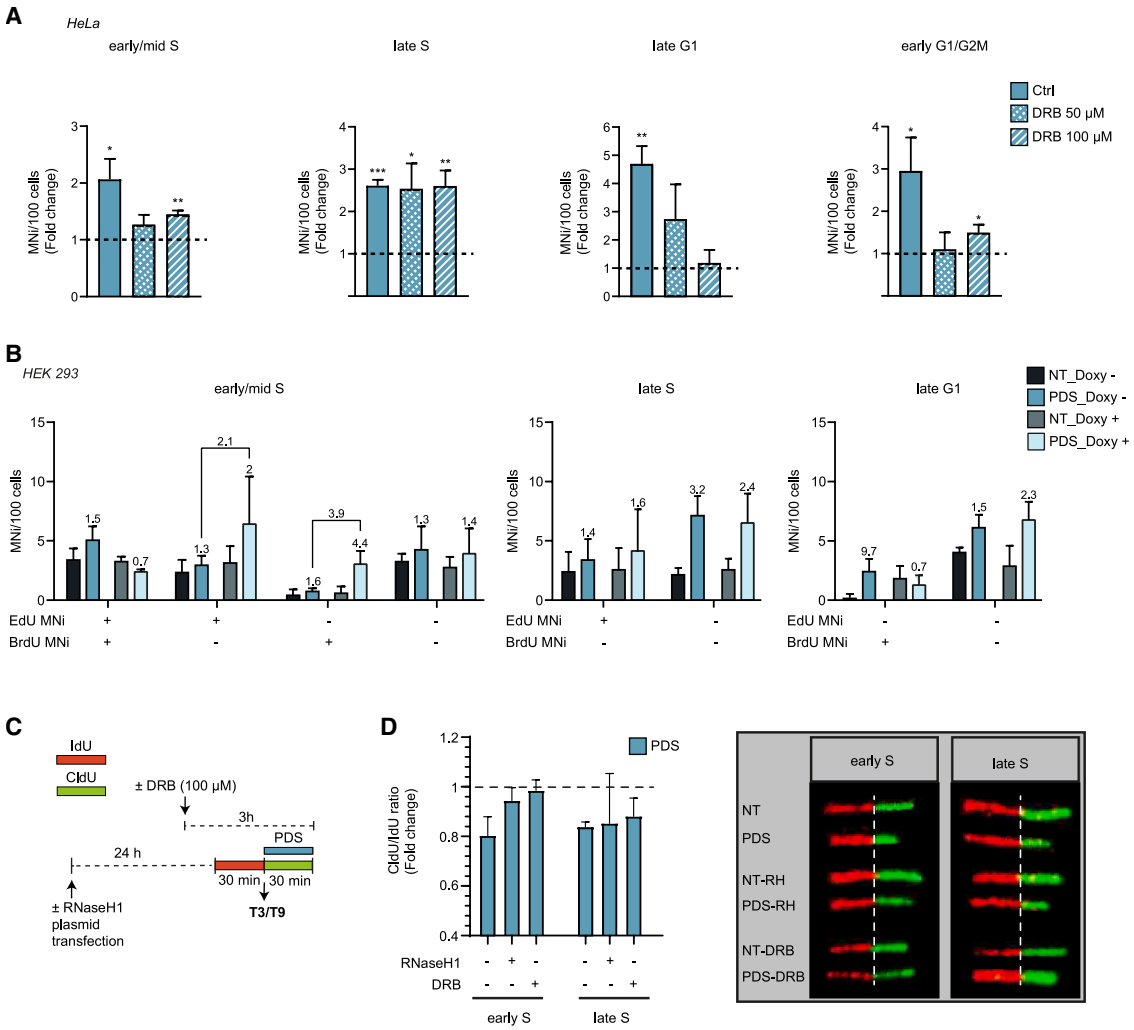

Figure 4. High transcription rates trigger G4-induced micronuclei and fork stalling during early/mid S and late G1 phases

(A) Micronuclei increase in EdU-BrdU-labeled HeLa cells treated or not with DRB. Micronuclei quantitation in PDS-treated vs. untreated samples is reported as fold change of MNi/100 cell. Dotted lines: control sample. Graphs show mean ± SEM, $n = 3$. Average analyzed cells: 250 (early/mid S), 70 (late S), 60 (late G1), and 300 (early G1/G2M).

(B) EdU-BrdU micronuclei quantitation in dual-pulse labeled HEK293 cells treated (Doxy+) or not (Doxy−) with doxycycline to overexpress TFIISm. Graphs show mean ± SEM, $n = 3$. Average analyzed cells: 250 (early/mid S), 70 (late S), and 90 (late G1).

(C) DNA fiber assay experimental scheme.

(D) RNaseH1 overexpression and DRB-mediated transcription inhibition effect on PDS-induced replication fork slowing in HeLa cells (left). Median values of CldU:IdU ratio of treated vs. control samples (dotted lines) reported as fold change. Bars show means ± SEM, $n = 2$. Average analyzed fibers: 150. Representative images of IdU-CldU tracts (right).

*$p < 0.05$, **$p < 0.01$, ***$p < 0.001$ (t test). See also Figure S4.

micronuclei using the dual-pulse labeling scheme (Figure 3A). We first silenced PrimPol with a specific small interfering RNA (siRNA) in HeLa cells at undetectable levels (Figure S5A, top). The lack of PrimPol did not reduce PDS-induced micronucleus levels in late G1 and early/mid S cells, whereas they were drastically reduced in late S cells (Figure 5A). We also investigated PrimPol role in wild-type (WT) and PrimPol gene knockout (KO) U2OS cells[47] (Figures 5B and S5A, bottom). In KO cells, we did not observe significant change in the level of PDS-induced micronuclei in late G1, early/mid S, and early G1/G2M phases (Figure 5B). However, PrimPol gene KO completely abrogated PDS-induced micronuclei in late S phase cells. This effect was rescued by PrimPol expression from a transfected vector (Figure 5B).

To assess PrimPol specificity for G4 structures, we then determined its role on camptothecin-induced micronuclei in the PrimPol KO cell model. The results clearly show that camptothecin did not induce micronuclei in late S also in another cell line and that camptothecin-induced micronuclei increase is not reduced by the absence of PrimPol, supporting its specific role in stabilized G4s at stalled replication forks in late S phase (Figure S5B).

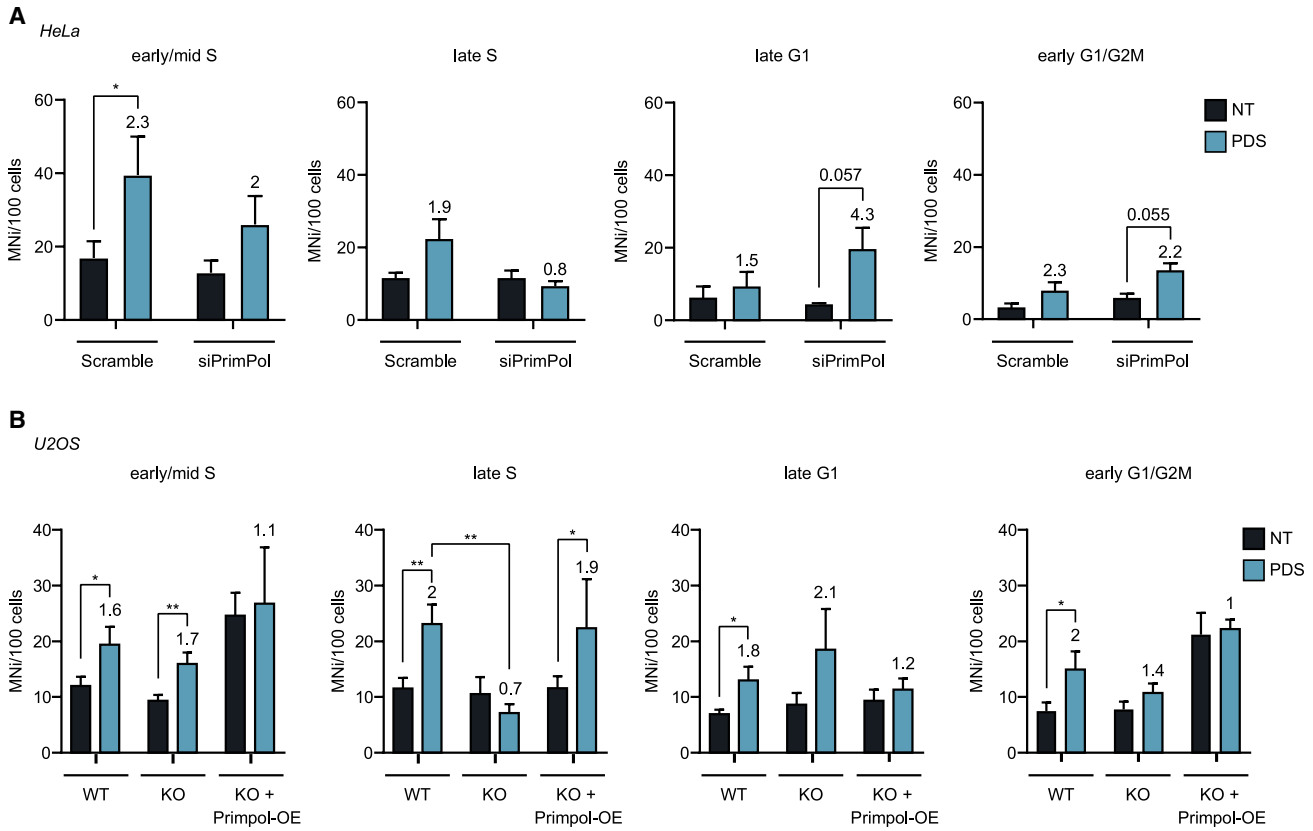

Figure 5. PrimPol promotes PDS-induced micronuclei exclusively in late S phase

(A) Micronuclei quantitation in EdU-BrdU-labeled HeLa cells transfected with scrambled (Scramble) or specific PrimPol siRNAs (siPrimPol) 48 h before EdU-BrdU and PDS treatments. Graphs show mean ± SEM, $n = 3$. Average number of analyzed cells is 200 (early/mid S), 80 (late S), 80 (late G1), and 350 (early G1/G2M). (B) Micronuclei increase in PrimPol WT (WT), PrimPol KO (KO), and PrimPol complemented (KO + PrimPol-OE) U2OS cells in early/mid S, late S, late G1, and early G1/G2M during PDS treatment. Graphs represent mean ± SEM ($n = 3$ and $n = 2$ for "WT/KO" and "KO + PrimPol-OE," respectively). Average analyzed cells: U2OS WT, 370 (early/mid S), 95 (late S), 60 (late G1), 430 (early G1/G2M); U2OS KO, 500 (early/mid S), 90 (late S), 110 (late G1), and 420 (early G1/G2M); U2OS complemented, 200 (early/mid S), 50 (late S), 80 (late G1), and 190 (early G1/G2M). PrimPol overexpression affects micronucleus levels in some untreated cells; however, the effect is not the same among different cell categories.

*$p < 0.05$, **$p < 0.01$, (t test). See also Figure S5.

Overall, results obtained in two cell models show that PrimPol activity is required for G4-induced micronuclei in late S only, in agreement with its higher expression and activity in late S phase.[48]

DNA Pol η contributes to the mechanism of micronuclei formation in a G-loop-dependent manner in early/mid S phase but independently from G-loops in late S phase

Although both camptothecin and PDS can induce TRCs,[27,40] the immediate consequence for DNA integrity is markedly different as camptothecin causes high levels of DSBs,[40] whereas PDS causes no DNA cleavage (Figures 2A–2D). Since re-priming or bypass may restart a stalled fork without inducing strand cuts, we wondered whether the TLS DNA Pol η is involved in G4-induced micronuclei in any cell-cycle phases.

Firstly, we silenced Pol η in HeLa cells (Figure 6A) and investigated micronuclei formation with the dual-pulse labeling scheme (Figure 3A). Pol η silencing itself could increase micronuclei formation in HeLa cells (Figure S6A, top) while it markedly reduced or abolished the micronuclei increase by stabilized G4s in all tested phases (Figures 6B and S6B, top). Similar data were obtained in WT U2OS cell line (Figures 6C, 6D, S6A, and S6B, bottom), therefore showing that Pol η activity has a role in the response to G4-induced stalled replication forks (Figures 4C and 4D), eventually leading to micronuclei formation. Next, we wondered whether Pol η effects were dependent on PrimPol. Hence, we silenced Pol η in PrimPol KO U2OS cells (Figures 6C, S6A, and S6B, bottom) and determined micronucleus levels upon PDS treatment. The lack of PrimPol does not affect Pol η effects in early/mid S, late G1, and early G1/G2M phases (Figures 6D and S6B, bottom), suggesting that Pol η only is required in late G1 and early/mid S phases. In addition, since either PrimPol or Pol η silencing can abolish micronuclei formation in late S, both PrimPol and Pol η activities are required during late S phase. We also assessed the effects of Pol η silencing on mitotic errors in HeLa cells. Consistently, Pol η silencing reduced anaphase bridges and lagging chromosomes (Figure S6C). Mitotic index was increased, while mitotic duration

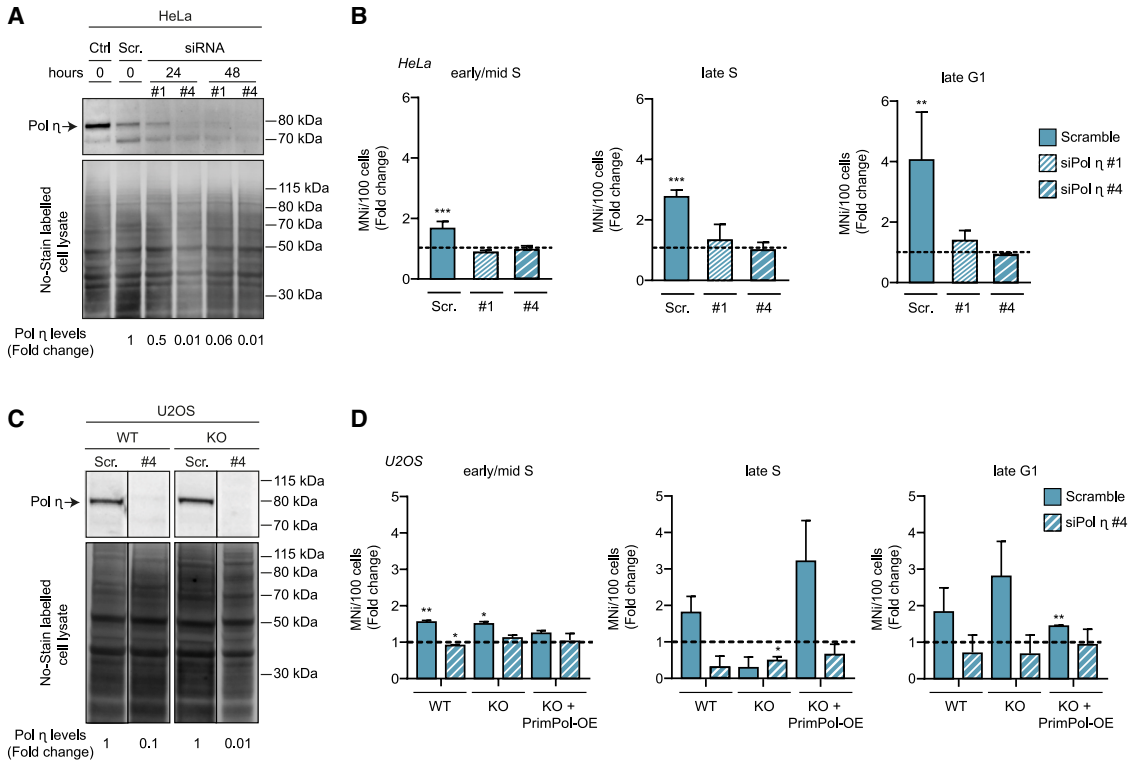

Figure 6. Pol η activity triggers G4-induced micronuclei in all cell-cycle phases

(A) Pol η immunoblot in HeLa cells not-transfected (Ctrl), transfected with a scrambled (Scr.), or transfected with two Pol η-specific siRNAs (#1 and #4) for 24 and 48 h before PDS treatment. Top and bottom, immunoblot and loading control, respectively. Expression levels in silenced (#1 and #4) vs. scrambled samples (Scr.) are reported as fold change.

(B) Micronuclei quantitation in dual-pulse labeled HeLa cells transfected with scrambled (Scr.) or Pol η-specific siRNAs (#1 and #4) 48 h prior to EdU-BrdU and PDS administration. Micronuclei quantitation in PDS-treated vs. untreated samples reported as fold change of MNi/100 cell. Dotted lines: control sample. Bars show mean ± SEM, $n = 3$. Average analyzed cells: 185 (early/mid S), 85 (late S), and 65 (late G1).

(C) Pol η immunoblot in U2OS PrimPol WT (WT) and U2OS PrimPol KO (KO) transfected with a scrambled (Scr.) or Pol η-specific siRNAs (#4) for 24 h. Top and bottom, immunoblot and loading control, respectively. Quantification of Pol η expression levels as in (A).

(D) Micronuclei increase in PrimPol WT (WT), PrimPol KO (KO), and PrimPol complemented (KO + PrimPol-OE) U2OS cells in early/mid S, late S, late G1, and early G1/G2M during PDS treatment. Cells were treated with a Pol η-specific siRNA (siPol η #4) 24 h prior to EdU-BrdU and PDS administration. Micronuclei quantitation in PDS-treated vs. control samples is reported as fold change of MNi/100 cells. Dotted lines: control sample. Average analyzed cells: 230 (early/mid S), 45 (late S), and 55 (late G1).

Graphs show mean ± SEM, $n = 2$. *$p < 0.05$, **$p < 0.01$, ***$p < 0.001$ (t test). See also Figure S6.

(Figure S6D) and labeled cell distribution (Figure S6E) were not affected by either Pol η silencing or PDS. Therefore, the reduction of mitotic errors and micronuclei was not due to a decrease in mitosis rates or duration. Since Pol η can have a role during early S phase at highly transcribed regions of early-replicating IZs,[49–51] we then investigated whether Pol η can affect PDS-induced TRCs at early vs. late S phases by using a proximity ligation assay (PLA) with antibodies specific for either PCNA (proliferating cell nuclear antigen) or RNAPII largest subunit (Figures 7A and S7A). We labeled S phase cells with EdU and distinguished early/mid S from late S phase from fluorescent spot patterns.[52] Firstly, stabilized G4s mainly increase TRC foci in early/mid S phase cells as the fold change was higher in those cells in comparison to late S cells (3.4 vs. 1.6, Figures 7A and 7B). In G1/G2M cells, we could see a low level of PLA signal, likely corresponding to cells at the G1/S boundary, and stabilized G4s increased this signal to a similar extent (Figures 7A and 7B). In cells depleted of Pol η, TRCs were reduced; nevertheless, the G4-dependent increase of TRCs was similar to that of control cells and was always specific for early/mid S phase cell category (Figures 7A and 7B). PCNA-PCNA PLA experiments showed that PCNA itself was reduced in nuclear chromatin of silenced-Pol η cells with respect to control cells (Figure S7B), suggesting that Pol η silencing-dependent reduction of PDS-induced TRCs is largely due to a reduction of the PCNA-PCNA signal, hence reduction of overall DNA synthesis (Figure S7B). Overall, stabilized G4s mainly induce TRCs in early/mid S phase, and Pol η increases the chance of TRCs likely favoring fork progression.[53]

Since R-loops have a role in the mechanism of micronuclei formation by G4 stabilization at late G1 and early/mid S phases, we then asked if Pol η can be recruited close to hybrids. First, we analyzed early-replicating regions for the extent of Pol η density using published datasets.[54] Pol η density was increased at early-replicating IZs enriched for stabilized

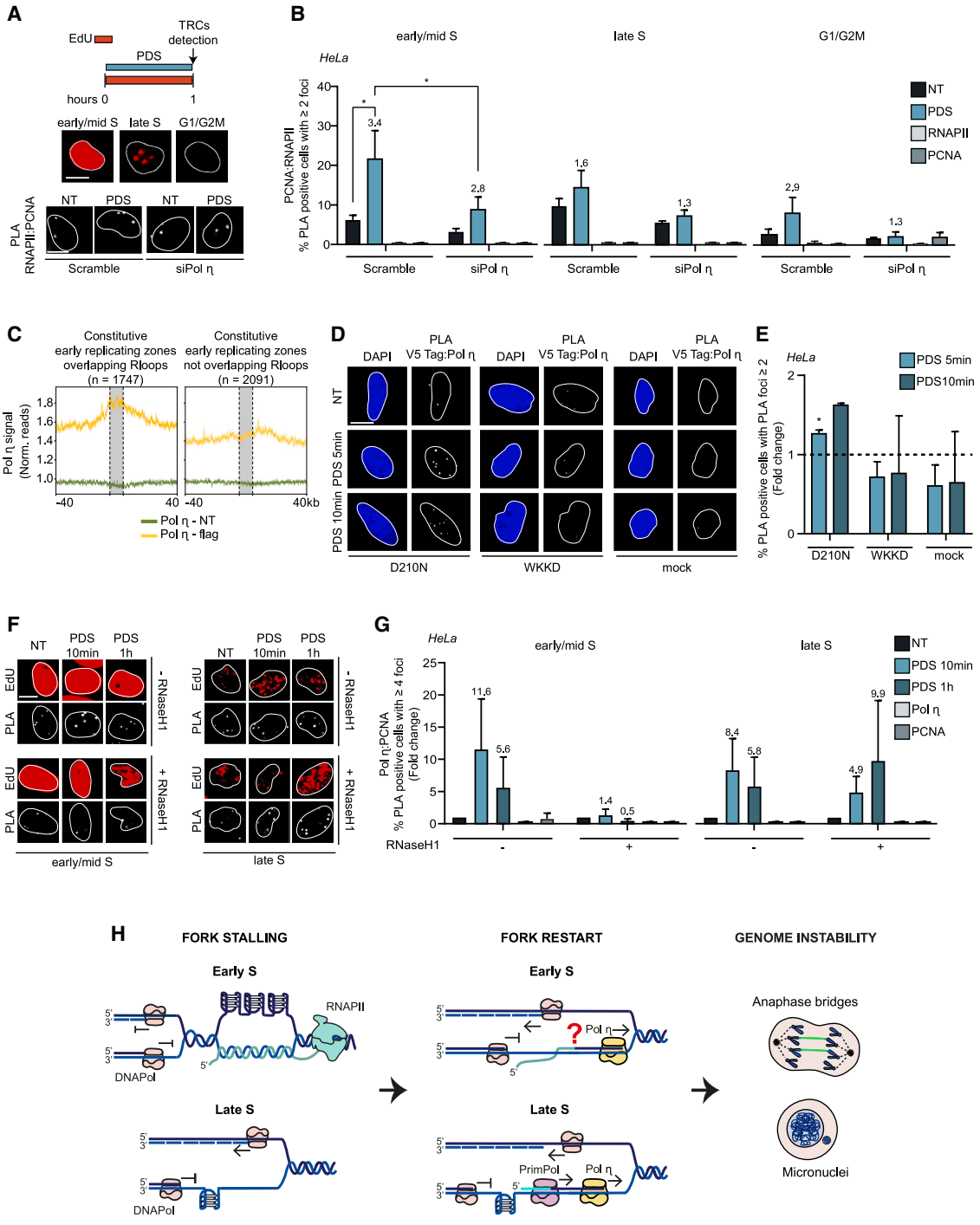

Figure 7. Pol η interacts with RNA:DNA hybrids at early replicating zones, increasing the chance of G4-induced TRCs

(A and B) PLA between PCNA and RNAPII. Experimental design (top) and representative images of EdU-labeled cells and PLA foci (bottom) (A). PLA foci in early/mid S, late S, and G1/G2M cells treated with a scrambled (Scramble) or Pol η siRNA#4 for 24 h prior to drug treatment (see Figure 6 A) (B). "RNAPII" and "PCNA": negative controls (indicated Ab only). Graphs show mean ± SEM, $n = 3$. Average analyzed cells: 150 (early/mid S), 40 (late S), and 300 (G1/G2M). *$p < 0.05$ (t test).
(C) Metaplot showing ChIP-seq mean normalized levels of Pol η[54] at constitutive early replicating zones that overlap an R-loop (left panel) or not (right panel). Gray-shaded area indicates the constitutive region (10 kb) in a window of +/− 40 kilobases (kb). ChIP-seq signals are reported as mean-normalized levels.
(D and E) PLA of V5-tagged RNaseH1 with Pol η. Representative images of DAPI and PLA foci in HeLa cells not overexpressing (mock) or overexpressing a modified RNAseH1 (D210N and WKKD) (D). Bar plots: ratio between 5 (PDS-5) or 10 (PDS-10) minutes PDS-treated vs. control cells (E). Dotted lines: control sample. Average analyzed cells: 300 (D210N), 260 (WKKD), and 160 (mock). Graphs show mean ± SEM, $n = 3$ and $n = 2$ for PDS-5 and PDS-10, respectively. *$p < 0.05$ (ratio t test on not normalized data).

(legend continued on next page)

G4-induced R-loops (see earlier text), whereas it was markedly lower in early-replicating IZs not enriched for R-loops (Figure 7C). Consistently, PLA data showed that Pol η is very close to stabilized G4-increased hybrids (Figures 7D, 7E, and S7C), suggesting an interaction between Pol η and hybrids. Next, we wondered if Pol η/PCNA interaction can be dependent on hybrids under our conditions, performing PLA experiments of Pol η/PCNA interaction with and without RNaseH1 overexpression. The findings showed that Pol η/PCNA interaction depends strongly on hybrids in early/mid S but not in late S phases (Figures 7F, 7G, S7D, and S7E). Thus, the results are consistent with the hypothesis that Pol η can interact with hybrids within replication forks stalled by G4-dependent collisions with transcription at highly transcribed genes in early-replicating IZs (Figure 7G).

DISCUSSION

G4 structures can affect replication at different levels. First, G4-promoting sequence motifs have been identified in conserved replication origins in mammals suggesting a regulation role in establishing the site of replication origin.[56,57] Second, G4 stabilization can cause the formation of G-loops at highly transcribed genes[2,3,20] leading to increased TRC frequency, stalled forks, and, eventually, DSBs.[20,31] Third, G4s in the strand template[33] can hinder the replication machinery leading to the activity of specific factors (helicases, PrimPol, or TLS polymerases) to recover DNA synthesis without strand cleavage.[58–60] Here, we provide evidence that genomic context affects the molecular events following G4 stabilization likely including the mode of replication fork stalling and recovery. Genomic regions rich in highly transcribed genes are replicated early during S phase and are preferentially located in chromatin compartment A or topologically associating domains of open chromatin.[61,62] In contrast, silenced genes and compact chromatin (compartment B) are preferentially replicated in late S.[61,62] Our results show that replication fork stalling and recovery mechanisms leading to micronuclei formation are different in early S vs. late S, likely due to chromatin organization and genomic functions. Fork stalling is due to G-loop-mediated TRCs and G4s in the template strand in early/mid S and late S, respectively (Figure 7H). In addition, the immediate response at stalled forks does not involve DNA breakage and includes different re-priming/bypass mechanisms, which can lead to chromosomal instability. Our hypothesis is that different modes of fork restart based on Pol η and/or PrimPol activities and dependent on the genomic context can avoid immediate DNA breakage at stalled forks, but at the expense of a risk of later mitotic chromosomal instability (Figure 7H). As G4 stabilization by PDS did not markedly retard cell-cycle progression (Figure 2), TLS-dependent fork restart can be a quick responsive mechanism at TRCs to maintain a proper replication speed.

G4 stabilization during different cell-cycle phases does not cause immediate DSBs, even though they trigger increased levels of micronuclei and mitotic errors. Nuclear G4s are stabilized by PDS rapidly, and G4 foci return close to control levels within 1 h,[20] showing that these structures are highly dynamic triggering subsequent molecular events in chromatin. In highly transcribed euchromatin regions, G4 stabilization triggers the formation of G-loops[20] (Figures 3C, 3D, and S3E), increasing the frequency of TRCs and stalled replication forks. Pol η is close to G4-induced hybrids and recruited at higher levels at early-replicating IZs with R-loops (Figures 7C–7E). Since Pol η can bind to a DNA/RNA hybrid and use the RNA as a primer adding dNTPs to its 3′ end,[63] Pol η may thus restart DNA synthesis downstream of DNA-RNA hybrids at stalled replication forks as a transcript annealed to the DNA template may provide a ready 3′ end for the re-priming activity[63] (Figure 7H). Such a Pol η activity downstream of TRC and hybrids (Figure 7H) agrees with the reported suppression of replication pausing.[53] Moreover, G4s in the template of leading strand replication are more prone to trigger instability in yeast,[64] consistent with Pol η-dependent re-priming in case of co-directional TRCs (Figure 7H). Therefore, Pol η can maintain a proper replication rate at the expense of an increased risk to induce chromosomal instability (Figure 7) and genetic variations at common fragile sites.[53] G4s trigger G-loop increases and TRC frequencies to a much-reduced extent, if any, at late-replicating heterochromatin regions (Figures 3B, 4A, 7A, and 7B). In these regions, G4s can likely stop an advancing fork when they form in the template strand.[28,33,58] Here, we propose that re-priming downstream of a G4 obstacle is due to the activity of both PrimPol and Pol η (Figure 7H), eventually leading to chromosomal instability at mitosis. We cannot exclude, however, the idea that re-priming activity based on other factors (helicase activity, DNA polymerase δ, or others)[60] can also occur without DNA breakage and later chromosomal instability.

G4 stabilization by PDS for a short time does not produce DNA cleavage, and re-priming/bypass activity can be an effective, quick response to fork stalling.[60] In case of long PDS treatments, DNA synthesis re-priming becomes less effective; therefore, other responses likely occur at stalled forks, including activation of nucleases and a full DNA damage response.[2,20,31] Although the immediate DNA cleavage outcome is markedly different between PDS and camptothecin (Figure 2),[40] both compounds induce hybrid-mediated TRCs at early replicating IZs (Figure 7B).[40] TFIIS, a factor that promotes transcription elongation by rescuing arrested RNAPIIs,[46,65,66] can reduce G4-induced micronuclei (Figures 4B and S4A). Thus, an arrested RNAPII may play a role in G4-induced TRCs and chromosomal instability. A backtracked RNAPII would make the transcript 3′ end free to anneal back to the template strand,[40,46] and then it would be readily available for Pol η re-priming downstream of a co-directional TRC (Figure 7H). However, the role of an arrested

(F and G) Pol η:PCNA PLA foci in early/mid S and late S HeLa cells, transiently transfected with an RNAseH1-expressing plasmid. Bar plots show Pol η:PCNA PLA foci fold change of treated vs. control cells. Graphs show mean ± SEM, $n = 3$. Average analyzed cells: 223 (early/mid) S and 26 (late S). Statistical significance was calculated by t test.

(H) Model of cell-cycle-specific mechanism of G4-mediated genome instability. The model can be similar for head-on TRCs with some adjustments. Other fork bypass mechanisms, in addition to re-priming, may be involved in this process.[55] See also Figure S7.

RNAPII in G4-induced chromosomal instability remains to be established in future studies.

Limitations of the study

Under our conditions of cell treatments with PDS for 1 h only, we have shown mechanisms which can immediately respond to stalled replication forks by stabilized G4s. However, we cannot exclude other mechanisms, dependent on DSBs, of G4-induced micronuclei when stabilized G4s last for longer periods. Additional mechanisms, such as nuclease-dependent recovery of replication fork arrest,[27] may resolve G4-induced collapsed replication forks. Moreover, our data cannot distinguish head-on from co-directional TRCs; therefore, the proposed model shows a co-directional TRC for clarity only (Figure 7H). Our findings show that Pol η- and/or PrimPol-mediated restart of forks stalled by G4 results in micronuclei formation. However, since we have not shown whether TLS polymerases can extend an RNA of G4-induced G-loops under our conditions, we cannot exclude that Pol η-dependent fork restart involves other enzyme activities, such as a bypass event with the use of the other nascent DNA strand as template. Lastly, since RHPS4 showed only a slight increase of MNi formation in early/mid S cells as compared with PDS and CX-5461, our data do not clarify whether chemical-specific patterns of stabilized G4s in living cells may differently affect micronuclei induction. Thus, future studies need to provide further mechanistic aspects of the proposed genome context-dependent mechanisms.

RESOURCE AVAILABILITY

Lead contact

Requests for further information, resources, and reagents should be directed to and will be fulfilled by the lead contact, Giovanni Capranico (giovanni.capranico@unibo.it).

Materials availability

This study did not generate new unique reagents.

Data and code availability

- This study did not generate new sequencing data. Accession numbers of sequencing data used in this study are listed in the key resources table.
- This paper does not report original code.
- Any additional information required to reanalyze the data reported in this paper is available from the lead contact upon request.

ACKNOWLEDGMENTS

We thank Dr. Alessandro Vindigni (Division of Oncology, Department of Medicine, Washington University in St. Louis, USA) for providing us the PrimPol antibody and wild-type (WT) and PrimPol gene knock-out (KO) U2OS cell lines, Dr. Julian E. Sale (Cancer Research UK, Cambridge, UK) for providing us with YFP-tagged PrimPol WT expressing vector, and Jesper Q. Svejstrup (CGEN, University of Copenhagen, Denmark) for the HEK293-TFIISm cell line. We acknowledge the Centre for Applied Biomedical Research (CRBA), University of Bologna, for technical support. We thank our lab colleagues for several interesting discussions.

This work was funded by AIRC (Associazione Italiana per la Ricerca sul Cancro, Milan, Italy) (IG 2019 - ID. 23032 project to G.C.). The research leading to these results has also received funding from the European Union - NextGenerationEU through the Italian Ministry of University and Research under PNRR - M4C2-I1.3 Project PE_00000019 "HEAL ITALIA" to G.C., CUP (J33C22002920006). The views and opinions expressed are those of the authors only and do not necessarily reflect those of the European Union or the European Commission. Neither the European Union nor the European Commission can be held responsible for them. R.C.D. is a recipient of an FIRC-AIRC postdoc fellowship for Italy (26701).

AUTHOR CONTRIBUTIONS

G.C. conceived the study, supervised the research, and secured fundings. S. P., F.G., and R.C.D. conducted wet lab experiments. M.R. analyzed genomic data. S.P. prepared the figures. G.C. wrote the manuscript with input from all authors. All authors read, discussed, and approved the final version of the manuscript.

DECLARATION OF INTERESTS

The authors declare no competing interests.

STAR★METHODS

Detailed methods are provided in the online version of this paper and include the following:

- KEY RESOURCES TABLE
- EXPERIMENTAL MODEL AND STUDY PARTICIPANT DETAILS
  - Cell lines
- METHOD DETAILS
  - Cell transfections
  - Immunofluorescence microscopy
  - Micronuclei assay
  - Mitotic errors detection
  - γH2AX detection
  - Proximity ligation assay (PLA)
  - Double thymidine block and DNA fiber assay
  - Comet assay
  - Image analysis and representation
  - Cytofluorimetry
  - Livecyte assay
  - Protein extraction and western blotting
  - Bioinformatic analysis
- QUANTIFICATION AND STATISTICAL ANALYSIS
  - Statistical analysis

SUPPLEMENTAL INFORMATION

Supplemental information can be found online at https://doi.org/10.1016/j.celrep.2025.115706.

Received: August 14, 2024
Revised: March 11, 2025
Accepted: April 25, 2025

REFERENCES

1. Bochman, M.L., Paeschke, K., and Zakian, V.A. (2012). DNA secondary structures: stability and function of G-quadruplex structures. Nat. Rev. Genet. *13*, 770–780. https://doi.org/10.1038/nrg3296.
2. Miglietta, G., Russo, M., and Capranico, G. (2020). G-quadruplex–R-loop interactions and the mechanism of anticancer G-quadruplex binders. Nucleic Acids Res. *48*, 11942–11957. https://doi.org/10.1093/nar/gkaa944.
3. Maizels, N., and Gray, L.T. (2013). The G4 Genome. PLoS Genet. *9*, e1003468. https://doi.org/10.1371/journal.pgen.1003468.
4. Cheung, I., Schertzer, M., Rose, A., and Lansdorp, P.M. (2002). Disruption of dog-1 in Caenorhabditis elegans triggers deletions upstream of guanine-rich DNA. Nat. Genet. *31*, 405–409. https://doi.org/10.1038/ng928.

5. Varshney, D., Spiegel, J., Zyner, K., Tannahill, D., and Balasubramanian, S. (2020). The regulation and functions of DNA and RNA G-quadruplexes. Nat. Rev. Mol. Cell Biol. *21*, 459–474. https://doi.org/10.1038/s41580-020-0236-x.

6. Balasubramanian, S., Hurley, L.H., and Neidle, S. (2011). Targeting G-quadruplexes in gene promoters: a novel anticancer strategy? Nat. Rev. Drug Discov. *10*, 261–275. https://doi.org/10.1038/nrd3428.

7. Carvalho, J., Mergny, J.L., Salgado, G.F., Queiroz, J.A., and Cruz, C. (2020). G-quadruplex, Friend or Foe: The Role of the G-quartet in Anticancer Strategies. Trends Mol. Med. *26*, 848–861. https://doi.org/10.1016/j.molmed.2020.05.002.

8. Kwon, M., Leibowitz, M.L., and Lee, J.H. (2020). Small but mighty: the causes and consequences of micronucleus rupture. Exp. Mol. Med. *52*, 1777–1786. https://doi.org/10.1038/s12276-020-00529-z.

9. Ke, Y., Huh, J.W., Warrington, R., Li, B., Wu, N., Leng, M., Zhang, J., Ball, H.L., Li, B., and Yu, H. (2011). PICH and BLM limit histone association with anaphase centromeric DNA threads and promote their resolution. EMBO J. *30*, 3309–3321. https://doi.org/10.1038/emboj.2011.226.

10. Orr, B., De Sousa, F., Gomes, A.M., Afonso, O., Ferreira, L.T., Figueiredo, A.C., and Maiato, H. (2021). An anaphase surveillance mechanism prevents micronuclei formation from frequent chromosome segregation errors. Cell Rep. *37*, 109783. https://doi.org/10.1016/j.celrep.2021.109783.

11. Jiang, H., and Chan, Y.W. (2024). Chromatin bridges: stochastic breakage or regulated resolution? Trends Genet. *40*, 69–82. https://doi.org/10.1016/j.tig.2023.10.004.

12. Zhang, C.Z., Spektor, A., Cornils, H., Francis, J.M., Jackson, E.K., Liu, S., Meyerson, M., and Pellman, D. (2015). Chromothripsis from DNA damage in micronuclei. Nature *522*, 179–184. https://doi.org/10.1038/nature14493.

13. Miglietta, G., Marinello, J., Russo, M., and Capranico, G. (2022). Ligands stimulating antitumour immunity as the next G-quadruplex challenge. Mol. Cancer *21*, 180. https://doi.org/10.1186/s12943-022-01649-y.

14. Miglietta, G., Russo, M., Duardo, R.C., and Capranico, G. (2021). G-quadruplex binders as cytostatic modulators of innate immune genes in cancer cells. Nucleic Acids Res. *49*, 6673–6686. https://doi.org/10.1093/nar/gkab500.

15. Reisländer, T., Groelly, F.J., and Tarsounas, M. (2020). DNA Damage and Cancer Immunotherapy: A STING in the Tale. Mol. Cell *80*, 21–28. https://doi.org/10.1016/j.molcel.2020.07.026.

16. MacDonald, K.M., Nicholson-Puthenveedu, S., Tageldein, M.M., Khasnis, S., Arrowsmith, C.H., and Harding, S.M. (2023). Antecedent chromatin organization determines cGAS recruitment to ruptured micronuclei. Nat. Commun. *14*, 556. https://doi.org/10.1038/s41467-023-36195-8.

17. Dvorkin, S., Cambier, S., Volkman, H.E., and Stetson, D.B. (2024). New frontiers in the cGAS-STING intracellular DNA-sensing pathway. Immunity *57*, 718–730. https://doi.org/10.1016/j.immuni.2024.02.019.

18. Long, Z.J., Wang, J.D., Xu, J.Q., Lei, X.X., and Liu, Q. (2022). cGAS/STING cross-talks with cell cycle and potentiates cancer immunotherapy. Mol. Ther. *30*, 1006–1017. https://doi.org/10.1016/j.ymthe.2022.01.044.

19. Wilson, J.T. (2024). Controlling the STING pathway to improve immunotherapy. Nat. Nanotechnol. *19*, 718–720. https://doi.org/10.1038/s41565-024-01637-x.

20. De Magis, A., Manzo, S.G., Russo, M., Marinello, J., Morigi, R., Sordet, O., and Capranico, G. (2019). DNA damage and genome instability by G-quadruplex ligands are mediated by R loops in human cancer cells. Proc. Natl. Acad. Sci. USA *116*, 816–825. https://doi.org/10.1073/pnas.1810409116.

21. Duquette, M.L., Handa, P., Vincent, J.A., Taylor, A.F., and Maizels, N. (2004). Intracellular transcription of G-rich DNAs induces formation of G-loops, novel structures containing G4 DNA. Genes Dev. *18*, 1618–1629. https://doi.org/10.1101/gad.1200804.

22. Chedin, F., and Benham, C.J. (2020). Emerging roles for R-loop structures in the management of topological stress. J. Biol. Chem. *295*, 4684–4695. https://doi.org/10.1074/jbc.REV119.006364.

23. García-Muse, T., and Loops Aguilera, A.R. (2019). From Physiological to Pathological Roles. Cell. *179*, 604–618. https://doi.org/10.1016/j.cell.2019.08.055.

24. Luna, R., Gómez-González, B., and Aguilera, A. (2024). RNA biogenesis and RNA metabolism factors as R-loop suppressors: a hidden role in genome integrity. Genes Dev. *10*, 504–527, Published online July. https://doi.org/10.1101/gad.351853.124.

25. Duardo, R.C., Guerra, F., Pepe, S., and Capranico, G. (2023). Non-B DNA structures as a booster of genome instability. Biochimie *214*, 176–192. https://doi.org/10.1016/j.biochi.2023.07.002.

26. Kotsantis, P., Segura-Bayona, S., Margalef, P., Marzec, P., Ruis, P., Hewitt, G., Bellelli, R., Patel, H., Goldstone, R., Poetsch, A.R., and Boulton, S.J. (2020). RTEL1 Regulates G4/R-Loops to Avert Replication-Transcription Collisions. Cell Rep. *33*, 108546. https://doi.org/10.1016/j.celrep.2020.108546.

27. Chappidi, N., Nascakova, Z., Boleslavska, B., Zellweger, R., Isik, E., Andrs, M., Menon, S., Dobrovolna, J., Balbo Pogliano, C., Matos, J., et al. (2020). Fork Cleavage-Religation Cycle and Active Transcription Mediate Replication Restart after Fork Stalling at Co-transcriptional R-Loops. Mol. Cell *77*, 528–541.e8. https://doi.org/10.1016/j.molcel.2019.10.026.

28. Isik, E., Shukla, K., Pospisilova, M., König, C., Andrs, M., Rao, S., Rosano, V., Dobrovolna, J., Krejci, L., and Janscak, P. (2024). MutSβ-MutLβ-FANCJ axis mediates the restart of DNA replication after fork stalling at cotranscriptional G4/R-loops. Sci. Adv. *10*, eadk2685. https://doi.org/10.1126/sciadv.adk2685.

29. Rao, S., Andrs, M., Shukla, K., Isik, E., König, C., Schneider, S., Bauer, M., Rosano, V., Prokes, J., Müller, A., and Janscak, P. (2024). Senataxin RNA/DNA helicase promotes replication restart at co-transcriptional R-loops to prevent MUS81-dependent fork degradation. Nucleic Acids Res. *52*, 10355–10369. https://doi.org/10.1093/nar/gkae673.

30. Andrs, M., Stoy, H., Boleslavska, B., Chappidi, N., Kanagaraj, R., Nascakova, Z., Menon, S., Rao, S., Oravetzova, A., Dobrovolna, J., et al. (2023). Excessive reactive oxygen species induce transcription-dependent replication stress. Nat. Commun. *14*, 1791. https://doi.org/10.1038/s41467-023-37341-y.

31. Rodriguez, R., Miller, K.M., Forment, J.V., Bradshaw, C.R., Nikan, M., Britton, S., Oelschlaegel, T., Xhemalce, B., Balasubramanian, S., and Jackson, S.P. (2012). Small-molecule–induced DNA damage identifies alternative DNA structures in human genes. Nat. Chem. Biol. *8*, 301–310. https://doi.org/10.1038/nchembio.780.

32. Schiavone, D., Jozwiakowski, S.K., Romanello, M., Guilbaud, G., Guilliam, T.A., Bailey, L.J., Sale, J.E., and Doherty, A.J. (2016). PrimPol Is Required for Replicative Tolerance of G Quadruplexes in Vertebrate Cells. Mol. Cell *61*, 161–169. https://doi.org/10.1016/j.molcel.2015.10.038.

33. Lee, W.T.C., Yin, Y., Morten, M.J., Tonzi, P., Gwo, P.P., Odermatt, D.C., Modesti, M., Cantor, S.B., Gari, K., Huang, T.T., and Rothenberg, E. (2021). Single-molecule imaging reveals replication fork coupled formation of G-quadruplex structures hinders local replication stress signaling. Nat. Commun. *12*, 2525. https://doi.org/10.1038/s41467-021-22830-9.

34. Ait Saada, A., Teixeira-Silva, A., Iraqui, I., Costes, A., Hardy, J., Paoletti, G., Fréon, K., and Lambert, S.A.E. (2017). Unprotected Replication Forks Are Converted into Mitotic Sister Chromatid Bridges. Mol. Cell *66*, 398–410.e4. https://doi.org/10.1016/j.molcel.2017.04.002.

35. Dhoonmoon, A., Nicolae, C.M., and Moldovan, G.L. (2022). The KU-PARP14 axis differentially regulates DNA resection at stalled replication forks by MRE11 and EXO1. Nat. Commun. *13*, 5063. https://doi.org/10.1038/s41467-022-32756-5.

36. Lemaçon, D., Jackson, J., Quinet, A., Brickner, J.R., Li, S., Yazinski, S., You, Z., Ira, G., Zou, L., Mosammaparast, N., and Vindigni, A. (2017). MRE11 and EXO1 nucleases degrade reversed forks and elicit

MUS81-dependent fork rescue in BRCA2-deficient cells. Nat. Commun. *8*, 860. https://doi.org/10.1038/s41467-017-01180-5.

37. Mijic, S., Zellweger, R., Chappidi, N., Berti, M., Jacobs, K., Mutreja, K., Ursich, S., Ray Chaudhuri, A., Nussenzweig, A., Janscak, P., and Lopes, M. (2017). Replication fork reversal triggers fork degradation in BRCA2-defective cells. Nat. Commun. *8*, 859. https://doi.org/10.1038/s41467-017-01164-5.
38. Chan, K.L., North, P.S., and Hickson, I.D. (2007). BLM is required for faithful chromosome segregation and its localization defines a class of ultrafine anaphase bridges. EMBO J. *26*, 3397–3409. https://doi.org/10.1038/sj.emboj.7601777.
39. Chan, Y.W., Fugger, K., and West, S.C. (2018). Unresolved recombination intermediates lead to ultra-fine anaphase bridges, chromosome breaks and aberrations. Nat. Cell Biol. *20*, 92–103. https://doi.org/10.1038/s41556-017-0011-1.
40. Duardo, R.C., Marinello, J., Russo, M., Morelli, S., Pepe, S., Guerra, F., Gómez-González, B., Aguilera, A., and Capranico, G. (2024). Human DNA topoisomerase I poisoning causes R loop–mediated genome instability attenuated by transcription factor IIS. Sci. Adv. *10*, eadm8196. https://doi.org/10.1126/sciadv.adm8196.
41. Macheret, M., and Halazonetis, T.D. (2018). Intragenic origins due to short G1 phases underlie oncogene-induced DNA replication stress. Nature *555*, 112–116. https://doi.org/10.1038/nature25507.
42. Walz, S., Lorenzin, F., Morton, J., Wiese, K.E., von Eyss, B., Herold, S., Rycak, L., Dumay-Odelot, H., Karim, S., Bartkuhn, M., et al. (2014). Activation and repression by oncogenic MYC shape tumour-specific gene expression profiles. Nature *511*, 483–487. https://doi.org/10.1038/nature13473.
43. Narain, A., Bhandare, P., Adhikari, B., Backes, S., Eilers, M., Dölken, L., Schlosser, A., Erhard, F., Baluapuri, A., and Wolf, E. (2021). Targeted protein degradation reveals a direct role of SPT6 in RNAPII elongation and termination. Mol. Cell *81*, 3110–3127.e14. https://doi.org/10.1016/j.molcel.2021.06.016.
44. Xu, H., Di Antonio, M., McKinney, S., Mathew, V., Ho, B., O'Neil, N.J., Santos, N.D., Silvester, J., Wei, V., Garcia, J., et al. (2017). CX-5461 is a DNA G-quadruplex stabilizer with selective lethality in BRCA1/2 deficient tumours. Nat. Commun. *8*, 14432. https://doi.org/10.1038/ncomms14432.
45. Phatak, P., Cookson, J.C., Dai, F., Smith, V., Gartenhaus, R.B., Stevens, M.F.G., and Burger, A.M. (2007). Telomere uncapping by the G-quadruplex ligand RHPS4 inhibits clonogenic tumour cell growth in vitro and in vivo consistent with a cancer stem cell targeting mechanism. Br. J. Cancer *96*, 1223–1233. https://doi.org/10.1038/sj.bjc.6603691.
46. Zatreanu, D., Han, Z., Mitter, R., Tumini, E., Williams, H., Gregersen, L., Dirac-Svejstrup, A.B., Roma, S., Stewart, A., Aguilera, A., and Svejstrup, J.Q. (2019). Elongation Factor TFIIS Prevents Transcription Stress and R-Loop Accumulation to Maintain Genome Stability. Mol. Cell *76*, 57–69.e9. https://doi.org/10.1016/j.molcel.2019.07.037.
47. Quinet, A., Tirman, S., Jackson, J., Šviković, S., Lemaçon, D., Carvajal-Maldonado, D., González-Acosta, D., Vessoni, A.T., Cybulla, E., Wood, M., et al. (2020). PRIMPOL-Mediated Adaptive Response Suppresses Replication Fork Reversal in BRCA-Deficient Cells. Mol. Cell *77*, 461–474.e9. https://doi.org/10.1016/j.molcel.2019.10.008.
48. Bailey, L.J., Teague, R., Kolesar, P., Bainbridge, L.J., Lindsay, H.D., and Doherty, A.J. (2021). PLK1 regulates the PrimPol damage tolerance pathway during the cell cycle. Sci. Adv. *7*, eabh1004. https://doi.org/10.1126/sciadv.abh1004.
49. Chakraborty, A., Tapryal, N., Islam, A., Sarker, A.H., Manohar, K., Mitra, J., Hegde, M.L., and Hazra, T. (2023). Human DNA polymerase η promotes RNA-templated error-free repair of DNA double-strand breaks. J. Biol. Chem. *299*, 102991. https://doi.org/10.1016/j.jbc.2023.102991.
50. Despras, E., Sittewelle, M., Pouvelle, C., Delrieu, N., Cordonnier, A.M., and Kannouche, P.L. (2016). Rad18-dependent SUMOylation of human specialized DNA polymerase eta is required to prevent under-replicated DNA. Nat. Commun. *7*, 13326. https://doi.org/10.1038/ncomms13326.
51. Vaziri, C., Rogozin, I.B., Gu, Q., Wu, D., and Day, T.A. (2021). Unravelling roles of error-prone DNA polymerases in shaping cancer genomes. Oncogene *40*, 6549–6565. https://doi.org/10.1038/s41388-021-02032-9.
52. Fu, H., Redon, C.E., Thakur, B.L., Utani, K., Sebastian, R., Jang, S.M., Gross, J.M., Mosavarpour, S., Marks, A.B., Zhuang, S.Z., et al. (2021). Dynamics of replication origin over-activation. Nat. Commun. *12*, 3448. https://doi.org/10.1038/s41467-021-23835-0.
53. Twayana, S., Bacolla, A., Barreto-Galvez, A., De-Paula, R.B., Drosopoulos, W.C., Kosiyatrakul, S.T., Bouhassira, E.E., Tainer, J.A., Madireddy, A., and Schildkraut, C.L. (2021). Translesion polymerase eta both facilitates DNA replication and promotes increased human genetic variation at common fragile sites. Proc. Natl. Acad. Sci. USA *118*, e2106477118. https://doi.org/10.1073/pnas.2106477118.
54. Tang, F., Wang, Y., Gao, Z., Guo, S., and Wang, Y. (2022). Polymerase η Recruits DHX9 Helicase to Promote Replication across Guanine Quadruplex Structures. J. Am. Chem. Soc. *144*, 14016–14020. https://doi.org/10.1021/jacs.2c05312.
55. Bétous, R., Rey, L., Wang, G., Pillaire, M.J., Puget, N., Selves, J., Biard, D.S.F., Shin-ya, K., Vasquez, K.M., Cazaux, C., and Hoffmann, J.S. (2009). Role of TLS DNA polymerases eta and kappa in processing naturally occurring structured DNA in human cells. Mol. Carcinog. *48*, 369–378. https://doi.org/10.1002/mc.20509.
56. Cayrou, C., Coulombe, P., Vigneron, A., Stanojcic, S., Ganier, O., Peiffer, I., Rivals, E., Puy, A., Laurent-Chabalier, S., Desprat, R., and Méchali, M. (2011). Genome-scale analysis of metazoan replication origins reveals their organization in specific but flexible sites defined by conserved features. Genome Res. *21*, 1438–1449. https://doi.org/10.1101/gr.121830.111.
57. Castaño, B.A., Schorer, S., Guo, Y., Calzetta, N.L., Gottifredi, V., Wiesmüller, L., and Biber, S. (2024). The levels of p53 govern the hierarchy of DNA damage tolerance pathway usage. Nucleic Acids Res. *52*, 3740–3760. https://doi.org/10.1093/nar/gkae061.
58. Sato, K., Martin-Pintado, N., Post, H., Altelaar, M., and Knipscheer, P. (2021). Multistep mechanism of G-quadruplex resolution during DNA replication. Sci. Adv. *7*, eabf8653. https://doi.org/10.1126/sciadv.abf8653.
59. van Schendel, R., Romeijn, R., Buijs, H., and Tijsterman, M. (2021). Preservation of lagging strand integrity at sites of stalled replication by Pol α-primase and 9-1-1 complex. Sci. Adv. *7*, eabf2278. https://doi.org/10.1126/sciadv.abf2278.
60. Marians, K.J. (2018). Lesion Bypass and the Reactivation of Stalled Replication Forks. Annu. Rev. Biochem. *87*, 217–238. https://doi.org/10.1146/annurev-biochem-062917-011921.
61. Pope, B.D., Ryba, T., Dileep, V., Yue, F., Wu, W., Denas, O., Vera, D.L., Wang, Y., Hansen, R.S., Canfield, T.K., et al. (2014). Topologically associating domains are stable units of replication-timing regulation. Nature *515*, 402–405. https://doi.org/10.1038/nature13986.
62. Takahashi, S., Miura, H., Shibata, T., Nagao, K., Okumura, K., Ogata, M., Obuse, C., Takebayashi, S.I., and Hiratani, I. (2019). Genome-wide stability of the DNA replication program in single mammalian cells. Nat. Genet. *51*, 529–540. https://doi.org/10.1038/s41588-019-0347-5.
63. Su, Y., Egli, M., and Guengerich, F.P. (2017). Human DNA polymerase η accommodates RNA for strand extension. J. Biol. Chem. *292*, 18044–18051. https://doi.org/10.1074/jbc.M117.809723.
64. Lopes, J., Piazza, A., Bermejo, R., Kriegsman, B., Colosio, A., Teulade-Fichou, M.P., Foiani, M., and Nicolas, A. (2011). G-quadruplex-induced instability during leading-strand replication. EMBO J. *30*, 4033–4046. https://doi.org/10.1038/emboj.2011.316.
65. Nudler, E. (2012). RNA Polymerase Backtracking in Gene Regulation and Genome Instability. Cell *149*, 1438–1445. https://doi.org/10.1016/j.cell.2012.06.003.
66. Noe Gonzalez, M., Blears, D., and Svejstrup, J.Q. (2021). Causes and consequences of RNA polymerase II stalling during transcript elongation. Nat.

Rev. Mol. Cell Biol. *22*, 3–21. https://doi.org/10.1038/s41580-020-00308-8.

67. Mourón, S., Rodriguez-Acebes, S., Martínez-Jiménez, M.I., García-Gómez, S., Chocrón, S., Blanco, L., and Méndez, J. (2013). Repriming of DNA synthesis at stalled replication forks by human PrimPol. Nat. Struct. Mol. Biol. *20*, 1383–1389. https://doi.org/10.1038/nsmb.2719.
68. Choi, J.H., and Pfeifer, G.P. (2005). The role of DNA polymerase η in UV mutational spectra. DNA Repair *4*, 211–220. https://doi.org/10.1016/j.dnarep.2004.09.006.
69. Gyori, B.M., Venkatachalam, G., Thiagarajan, P.S., Hsu, D., and Clement, M.V. (2014). OpenComet: An automated tool for comet assay image analysis. Redox Biol. *2*, 457–465. https://doi.org/10.1016/j.redox.2013.12.020.
70. Li, H., and Durbin, R. (2009). Fast and accurate short read alignment with Burrows–Wheeler transform. Bioinformatics *25*, 1754–1760. https://doi.org/10.1093/bioinformatics/btp324.
71. Danecek, P., Bonfield, J.K., Liddle, J., Marshall, J., Ohan, V., Pollard, M.O., Whitwham, A., Keane, T., McCarthy, S.A., Davies, R.M., and Li, H. (2021). Twelve years of SAMtools and BCFtools. GigaScience *10*, giab008. https://doi.org/10.1093/gigascience/giab008.
72. Ramírez, F., Ryan, D.P., Grüning, B., Bhardwaj, V., Kilpert, F., Richter, A.S., Heyne, S., Dündar, F., and Manke, T. (2016). deepTools2: a next generation web server for deep-sequencing data analysis. Nucleic Acids Res. *44*, W160–W165. https://doi.org/10.1093/nar/gkw257.
73. Quinlan, A.R., and Hall, I.M. (2010). BEDTools: a flexible suite of utilities for comparing genomic features. Bioinformatics *26*, 841–842. https://doi.org/10.1093/bioinformatics/btq033.
74. Wickham, H. (2016). Ggplot2 (Springer International Publishing). https://doi.org/10.1007/978-3-319-24277-4.
75. Bizard, A.H., Nielsen, C.F., and Hickson, I.D. (2018). Detection of Ultrafine Anaphase Bridges. Methods Mol. Biol. *1672*, 495–508. https://doi.org/10.1007/978-1-4939-7306-4_33.
76. Schwab, R.A.V., and Niedzwiedz, W. (2011). Visualization of DNA Replication in the Vertebrate Model System DT40 using the DNA Fiber Technique. J. Vis. Exp. *56*, e3255. https://doi.org/10.3791/3255.

STAR★METHODS

KEY RESOURCES TABLE

REAGENT or RESOURCE	SOURCE	IDENTIFIER
Antibodies		
BrdU Monoclonal Antibody (MoBU-1), Alexa Fluor™ 488	Thermo Fisher Scientific	Cat# B35130; RRID: AB_2536434
BrdU, clone B44	BD Biosciences	Cat# 347580; RRID:AB_10015219
Rat Anti-BrdU Monoclonal Antibody, Unconjugated, Clone BU1/75 (ICR1)	Abcam	Cat# ab6326; RRID:AB_305426
Goat anti-Mouse IgG (H + L) Cross-Adsorbed Secondary Antibody, Alexa Fluor™ 488	Thermo Fisher Scientific	Cat# A11001; RRID: AB_2534069
Anti-DYKDDDK Antibody, Unconjugated	Cell Signaling Technology	Cat# 2368; RRID: AB_2217020
Anti-PICH, clone 142-26-3	Millipore	Cat# 04–1540; RRID: AB_11210090
RPA70 antibody [EPR3472]	Abcam	Cat# ab79398; RRID:AB_1603759
Anti-phospho-Histone H2A.X (Ser139) Antibody, clone JBW301	Millipore	Cat# 05–636; RRID:AB_309864
Mouse Anti-Human PCNA (PC11) Monoclonal, Unconjugated, Clone Pc11	Santa Cruz Biotechnology	Cat# sc-53407; RRID:AB_630090
PCNA antibody - Proliferation Marker	Abcam	Cat# ab18197; RRID:AB_444313
Anti-RNAPII largest subunit antibody (Pol II, H-224)	Santa Cruz Biotechnology	Cat# sc-9001; RRID:AB_2268548
Mouse Anti-Human POL H (B-7) Monoclonal, Unconjugated, Clone B-7	Santa Cruz Biotechnology	Cat# sc-17770; RRID:AB_2167007
Rabbit Anti-V5 tag Polyclonal Antibody, Unconjugated	Abcam	Cat# ab15828; RRID:AB_443253
Goat Anti-Mouse IgG (H + L) Highly Cross-adsorbed Antibody, Alexa Fluor 568 Conjugated	Thermo Fisher Scientific	Cat# A11031; RRID:AB_144696
Goat anti-Rat IgG (H + L) Highly Cross-Adsorbed Secondary Antibody, Alexa Fluor™ Plus 488	Thermo Fisher Scientific	Cat# A48262; RRID:AB_2896330
Goat anti-mouse IgG-HRP Polyclonal, Hrp Conjugated	Santa Cruz Biotechnology	Cat# sc-2005; RRID:AB_631736
Goat Anti-Rabbit IgG H&L (HRP)	Abcam	Cat# ab205718; RRID:AB_2819160
Phospho-Histone H2A.X (Ser139) (20E3) Rabbit mAb	Cell Signaling Technology	Cat# 9718; RRID:AB_2118009
Phospho-Chk2 (Thr68) (C13C1) Rabbit mAb	Cell Signaling Technology	Cat# 2197; RRID:AB_2080501
Anti-Primpol homemade	Gift by A. Vindigni (Division of Oncology, Department of Medicine, Washington University in St. Louis, USA) Mourón et al.[67]	N/A
Bacterial and virus strains		
E. coli DH5α		N/A
Chemicals, peptides, and recombinant proteins		
Bromodeoxyuridine (BrdU)	Thermo Fisher Scientific	Cat# 23151
Camptothecin (CPT)	Merck	Cat# C9911
5-Chloro-2′-deoxyuridine (CldU)	Merck	Cat# C6891
CX-5461	Merck	Cat# 505016
Doxycycline	Merck	Cat# A7802
5,6-dichloro-1-beta-D-ribofuranosylbenzimidazole (DRB)	Merck	Cat# D1916

(*Continued on next page*)

Continued

REAGENT or RESOURCE	SOURCE	IDENTIFIER
5-Iodo-2′-deoxyuridine (IdU)	Merck	Cat# I7125
ML216	MedChemExpress	Cat# HY-12342
Nocodazole	Merck	Cat# M1404
Pyridostatin (PDS)	Selleckchem	Cat# S7444
PFM01	Merck	Cat# SML1735
PFM39	Merck	Cat# SML1839
RHPS4	Selleckchem	Cat# S8118
RO3306	Selleckchem	Cat# S7747
Thymidine	Merck	Cat# T1895
Critical commercial assays		
Click-iT™ EdU Cell Proliferation Kit for Imaging, Alexa Fluor™ 594 dye	Thermo Fisher Scientific	Cat# C10339
Click-iT™ EdU Cell Proliferation Kit for Imaging, Alexa Fluor™ 647 dye	Thermo Fisher Scientific	Cat# C10340
Duolink *In Situ* PLA Kit	Merck	Cat# DUO92101
Deposited data		
Genomic DRIP-seq	De Magis et al.[20]	GEO: GSE115957
GRO-seq	Walz et al.[42]	GEO: GSE44672
pS2RNAPII ChIP-seq	Narain et al.[43]	GEO: GSE162264
Pol η ChIP-seq	Tang et al.[54]	GEO: GSE203015
Experimental models: Cell lines		
HeLa	ATCC	N/A
HeLa D210N	Duardo et al.[40]	N/A
HeLa WKKD	Duardo et al.[40]	N/A
Hek293T-TFIISm	Gift by J. Q. Svejstrup (CGEN, University of Copenhagen, Denmark)	Previously characterized and validated in Zatreanu et al.[46]
U2OS WT	Gift by A. Vindigni (Division of Oncology, Department of Medicine, Washington University in St. Louis, USA)	Previously characterized and validated in Quinet et al.[47]
U2OS Primpol KO	Gift by A. Vindigni (Division of Oncology, Department of Medicine, Washington University in St. Louis, USA)	Previously characterized and validated in Quinet et al.[47]
U2OS_RH	De Magis et al.[20]	N/A
Oligonucleotides		
siRNA_BRCA2	Qiagen	Cat# sI02653595
siRNA_PrimPol	Ambion-Thermo Fisher	Cat# s47417
siRNA_Pol η #1	Choi et al.[68]	N/A
siRNA_Pol η #4	Choi et al.[68]	N/A
Scramble siRNA	Ambion-Thermo Fisher	Cat# #4390846
Recombinant DNA		
pcDNA3-RNaseH1	Gift by F. Chedin (University of California Davis)	N/A
YFP-tagged PrimPol WT expressing vector	Gift by J. Sale (MRC Laboratory of Molecular Biology, Francis Crick Avenue, Cambridge, CB2 0QH, UK)[32]	N/A
Software and algorithms		
Prism 9	GraphPad Software	N/A
ImageLab	BioRad	N/A
BioRender	https://www.biorender.com/	N/A
ImageJ (Fiji)	GitHub	https://imagej.net/software/fiji/

(*Continued on next page*)

Continued

REAGENT or RESOURCE	SOURCE	IDENTIFIER
Open Comet	Gyori et al.[69]	https://cometbio.org/
CytExpert Software	Beckman Coulter	https://www.beckman.com/flow-cytometry/research-flow-cytometers/cytoflex/software
Phasefocus analyze Software	https://www.phasefocus.com/	v3.12.2
Bwa	Li et al.[70]	version 0.7.17
Samtools	Danecek et al.[71]	version 0.15
Picard	Broad Institute	version 2.26.11
Deeptools	Ramírez et al.[72]	version 3.5.1
Bedtools	Quinlan et al.[73]	version 2.30.0
R base	R Core Team	version 4.4.0
ggplot	Wickham[74]	version 3.5.1

EXPERIMENTAL MODEL AND STUDY PARTICIPANT DETAILS

Cell lines

Human cancer HeLa cell line was purchased from ATCC (LGC Standards S.r.l., Milan, Italy). HeLa cells were cultured in Dulbecco's Modified Eagle Medium (DMEM, Thermo Fisher Scientific, #21969035) supplemented with 10% heat inactivated FBS (Thermo Fisher Scientific, #A5256701). HeLa cells stably expressing a catalytically inactive RNaseH1 (D210N) or a catalytically and DNA binding inactive RNaseH1 (WKKD) were previously generated in our laboratory.[40] These cell lines were cultured in DMEM supplemented with 10% heat inactivated FBS, 100 μg/mL penicillin-streptomycin (Thermo Fisher Scientific, #15140122) and 300 μg/mL Hygromycin B (Thermo Fisher Scientific, #10687010). HEK293-TFIISm cell line, which stably express a doxycycline-inducible full-length mutant of TFIIS (TCEA1),[46] was kindly supplied by Jesper Q. Svejstrup (CGEN, University of Copenhagen, Denmark). HEK293-TFIISm cells were cultured in DMEM supplemented with 10% FBS tetracycline-free (Takara, #631106), 100 μg/mL penicillin-streptomycin, 250 μg/mL zeocin (Thermo Fisher Scientific, #R25001) and 5 μg/mL blasticidin (Thermo Fisher Scientific, #R210-01). All the cell lines mentioned were cultured in humidified incubator at 5% of CO_2 and 37°C. To induce TFIISm overexpression, 80 ng/mL (0.18 μM) doxycycline were added for 48h to the same medium without antibiotics. PrimPol wild-type (WT) and PrimPol gene knockout (KO) U2OS cell lines[47] were kindly supplied by Vindigni A. (Division of Oncology, Department of Medicine, Washington University in St. Louis, USA) and were cultured in DMEM supplemented with 10% FBS and 100 μg/mL penicillin-streptomycin. U2OS-RH cells have been previously generated by transfecting U2OS cell line with pLVX-Tight-Puro-RH-Flag and pLVX-EF1a-Tet3G-Hygro plasmids to overexpress an exogenous RNase H1.[20] This cell line was maintained by adding 10% FBS tetracycline-free, 100 μg/mL penicillin-streptomycin, 1.5 μg/mL puromycin (Merck, #P8833) and 500 μg/mL hygromycin B to DMEM medium. RNaseH1 overexpression was induced, 24 h after seeding, by adding 2 μg/mL (4.5 μM) doxycycline for 48 h to the same medium without hygromycin and puromycin. Cell lines were routinely tested for mycoplasma contamination (Merck) and identity by STR (BMR genomics).

METHOD DETAILS

Cell transfections

To overexpress RNaseH1 in HeLa and U2OS cells, after 24 h from seeding, cells were transiently transfected with 2 μg of pcDNA3-RNaseH1 (gently furnished by F. Chedin) by using Lipofectamine 2000 (ThermoFisher Scientific, #11668027) with a ratio plasmid (μg): Lipofectamine 2000 (μL) of 1:2. To rescue PrimPol expression in U2OS PrimPol KO cells, after 24 h from seeding, cells were transiently transfected with 2 μg of YFP-tagged PrimPol WT expressing vector[32] (gently furnished by J. Sale) by using the same experimental conditions described above. Plasmid transfections were carried out on cell cultures 24 h before drug treatments. pcDNA3-RNaseH1 and YFP-tagged PrimPol WT plasmids were purified by using miniprep kit (Macherey Nagel, #740588.50) from *Escherichia coli* DH5α cells grown in LB medium with 100 μg/μL ampicillin or 25 μg/mL blasticidin respectively. HeLa and U2OS cells were transfected with pre-designed 20 nM scramble siRNA (ID #4390846, Ambion-Thermo Fisher), 20 nM siRNA against BRCA2 (ID #sI02653595, Qiagen)[20] and 20 nM PrimPol (ID# s47417 Ambion-Thermo Fisher), or with 60 nM custom siRNAs against Pol η[68] (siRNA#1 correspond to site 1 and siRNA#4 to site 4) by using RNAimax (Invitrogen, #13778075) according to datasheet instructions.

Immunofluorescence microscopy

For all imaging experiments, cells were seeded at low density on glass coverslips in six-well plates and allowed to attach. Drug treatments, plasmid and/or siRNAs transfections were performed directly on the cells on the coverslips.

Micronuclei assay

Micronuclei detection was carried out following the protocol already published in.[40] In brief, cells were treated with 10 μM PDS (Selleckchem, #S7444), 8 μM RHPS4 (Selleckchem, #S8118), 8 μM CX5461 (Merck Millipore, #505016) or 10 μM CPT (Merck, #C9911) for 1 h. To verify transcription dependence, cells were treated with 50 μM or 100 μM 5,6-dichloro-1-beta-D-ribofuranosylbenzimidazole (DRB) (Merck, #D1916) for 90 min before, during, and 1 h after PDS treatment (total 3 h). To distinguish cells in S phase, cells were treated with 10 μM EdU for 30 min before, during, and 1 h after the treatment making a total incubation period of 2.5 h. For a more precise subclassification of cells in the different phases of the cell cycle, 10 μM BrdU was administrated immediately after EdU for an additional 2.5 h. After EdU/BrdU removal, cells were rinsed with 1X PBS (137 mM NaCl, 10 mM Na_2HPO_4*$7H_2O$, 1.8 mM KH_2PO_4) and left in drug-free medium until the next mitosis (~24 h from drug removal). Then, cells were fixed with 4% formaldehyde, permeabilized with 1X PBS-0.5% Triton X-100 (Merck, #T8787) and subsequently labeled for EdU alone or for both EdU and BrdU staining. EdU staining was performed by using Click-iT EdU Assay (Thermo Fisher Scientific, #C10339) according to manufacturing instructions, while BrdU and DAPI staining were carried out as described in.[40] Briefly, a denaturation step before EdU staining was performed by incubating cells with 4 N of HCl at 25°C for 8 min. After two washes with 1X PBS, cells were incubated for 5 min in phosphate/citric acid (pH 7.4) (0.2 M Na_2HPO_4 and 0.1 M citric acid) followed by four additional washes: two with 1X PBS and two with 1X PBS containing 3% bovine serum albumine (BSA, Merck, #A4503). Cells were then labeled with EdU for 30 min. After two washes with 1X PBS-3% BSA cells were blocked with 1X PBS-3% BSA for 1 h at room temperature (RT) and incubated overnight (O/N) at 4°C with an anti-BrdU antibody (Thermo Fisher Scientific, #B35130) diluted 1:200 in blocking buffer with 0.1% Triton X-100. Cells were then incubated for 1 h at RT with an anti-mouse Alexa Fluor 488 secondary antibody (Thermo Fisher Scientific, #A11001) diluted 1:500 in 1X PBS-3% BSA. Following incubation, slides were washed with 1X PBS-3% BSA and then stained with DAPI (3.3 ng/μL in water) for 30 min. A final water wash was performed before mounting the slides with Mowiol and placing then upside down on microscope slides. During micronuclei analysis in U2OS-RH cells, RNaseH1 overexpression was assessed via immunofluorescence using the anti-DYKDDDK antibody (Cell Signaling Technology, #2368) targeting the FLAG Tag fused to the enzyme. The antibody was diluted 1:800 in 1X PBS-2% BSA. Further details regarding FLAG Tag staining are provided in.[40]

Mitotic errors detection

To investigate the dependence of fine bridges on R-loops, HeLa cells were seeded at a density of $2.5x10^6$ cells *per* T75 flask and transiently transfected with an RNAseH1 expressing plasmid for 24 h prior to EdU/BrdU and PDS treatments. To assess the dependence of fine bridges and lagging chromosomes on Pol η, HeLa cells were seeded at a density of $2.5x10^6$ cells *per* T75 flask and transfected with a scramble siRNA or a Pol η specific siRNA (siRNA#4) for 24 h before PDS treatment. For all other experiments, HeLa and U2OS cells were seeded at a density of 10^6 cells *per* T25 flask. After 24 h, cells were treated with 10 μM PDS for 1 h. To distinguish cells that were in S phase during drug treatments, cells were incubated with 10 μM EdU as detailed in micronuclei section. For a more precise subclassification of cells in the different phases of the cell cycle, 10 μM BrdU was administrated immediately after EdU for an additional 2.5 h. For anaphase bridges and lagging chromosomes detection, after EdU/BrdU administration cells were incubated with 0.16 μM (50 ng/mL) nocodazole for 20 h. At the end of nocodazole treatment, G2/M cells were collected by mitotic shake-off and released in fresh medium in 35 mm dishes containing a 24*24 mm poly-L-lysine coated cover glass for an additional 50 min. For nucleoplasmic bridges and micronuclei detection, upon EdU administration, cells were incubated for 16 h with 9 μM CDK1-i (RO3306). After RO3306 administration, G2 cells were released into fresh medium in presence or not of 25 μM BLM-i (ML216) for 30 min, allowing mitotic cells to progress to the M phase. Then, cells were collected by mitotic shake-off and released into fresh medium with or without 25 μM ML216 for an additional 50 min or 150 min depending on the detection of anaphase bridges or micronuclei, respectively. After collection, mitotic cells were fixed for 15 min with PTEMF buffer (20 mM PIPES pH 6.8, 1 mM $MgCl_2$, 10 mM EGTA, 0.4% Triton X-100 and 8% paraformaldehyde) at RT, rinsed with 1X PBS and then incubated O/N at 4°C in a blocking solution of 3% BSA in 1X PBS-0.5% Triton X-100.[75] EdU, BrdU and DAPI staining were carried out as described in micronuclei section, except for the denaturation step. Before EdU staining, anaphase cells were incubated with 4 N of HCl at 25°C for 20 min. Primary antibody incubation was carried out O/N at 4°C by using an anti-PICH (Millipore, #04–1540) diluted 1:100 or an anti-RPA70 antibody (Abcam, #ab79398) diluted 1:750 in blocking buffer. The secondary antibody incubation was performed for 1 h using an anti-mouse Alexa Fluor 488 (Thermo Fisher Scientific, #A11001) diluted 1:1000 in blocking buffer. After each primary or secondary antibody incubation, the slides were washed with a 1X PBS-3% BSA solution. DAPI staining was performed as previously described[40] and as detailed in micronuclei section.

γH2AX detection

Immunofluorescence assay for γH2AX detection was conducted following the protocol described in.[40] Briefly, after treatment with PDS and EdU (see micronuclei assay section), fixed HeLa cells were first stained for EdU and subsequently for Ser139-phosphorilated H2AX using the anti-γH2AX antibody (Millipore, #05–636) diluted 1:1000 in 1X PBS-1% BSA. Following primary antibody incubation, cells were incubated with an anti-mouse Alexa Fluor 488 secondary antibody (Thermo Fisher Scientific, #A11001) diluted 1:1000 in 1X PBS-1% BSA.

Proximity ligation assay (PLA)

Proximity ligation assay (PLA) was carried out by using the Duolink *In Situ* PLA Kit (Merck, #DUO92101-1KT) according to datasheet instructions. The procedure has already been described in.[40] In brief, 2.5 x 10^5 HeLa cells were seeded in 35 mm dishes containing 18*18 mm glass slides. For PLA assay between PCNA and RNAPII, after 24 h from seeding, cells were treated with 10 μM PDS and with 10 μM EdU for 1 h. PLA foci were determined at the end of EdU labeling. Early/mid S from late S phase cells were distinguished by means of fluorescent spot patterns [52]. At the end of PDS and EdU treatments, cells were fixed with formaldehyde 4% and permeabilized with 1X PBS-0.1% Triton X-100. Cells were incubated O/N at 4°C with anti-Proliferating Cell Nuclear Antigen antibody (anti-PCNA, Ab PC11, sc-53407) diluted 1:100 and Anti-RNAPII largest subunit antibody (Ab H-224, sc-9001) diluted 1:200. For PLA assay between RNaseH1 and Polymerase η (Pol η), HeLa D210N, HeLa WKKD or HeLa (mock) cell lines were treated with 10 μM PDS for 5 min or 10 min. Next, cells were fixed with a solution of 4% formaldehyde methanol-free and CSK buffer (100 nM NaCl; 300 mM Sucrose; 3 mM $MgCl_2$; 10 mM PIPES pH 6.8; 1 mM EGTA; 0.2% Triton; 1X protease inhibitor cocktail, Thermo Fisher Scientific, #78428). Cells were incubated O/N at 4°C with anti-Polymerase η antibody (Pol H, B-7, sc-17770) diluted 1:150 and Anti-Tag-V5 antibody (Abcam, ab15828) diluted 1:2000. For PLA assay between PCNA and PCNA, treatments were performed as described for PCNA:RNAPII PLA. Cells were then fixed with 4% formaldehyde in CSK buffer and permeabilized with 1X PBS-0.5% Triton X-100. O/N incubation at 4°C was carried out with anti-Proliferating Cell Nuclear Antigen antibody (anti-PCNA, Ab PC11, sc-53407) diluted 1:100 and anti-Proliferating Cell Nuclear Antigen antibody (anti-PCNA, Ab18197) diluted 1:800. Early/mid S phase cells were distinguished from late S phase cells based on fluorescent spot patterns.[52] For PLA assay between Pol η and PCNA, cells were transfected with an RNaseH1 expressing plasmid for 24 h after seeding, followed by treatment with 10 μM PDS for 10 min or 1 h, and 10 μM EdU for 1 h. Cells were then fixed as described above for PCNA:PCNA PLA and incubated O/N at 4°C with anti-Polymerase η antibody (Pol H, B-7, sc-17770) diluted 1:150 and anti-Proliferating Cell Nuclear Antigen antibody (anti-PCNA, Ab18197) diluted 1:800. Early/mid S from late S phase cells were again distinguished using fluorescent spot patterns.[52] Cells were observed with Nikon A1R Confocal Microscope (Eclipse Ti2). PLA positive cells were analyzed by using ImageJ software (analysis protocol for foci count available at https://microscopy.duke.edu/guides/count-nuclear-foci-ImageJ).

Double thymidine block and DNA fiber assay

Synchronization in S phase has been performed by using the double thymidine block protocol. Specifically, cells were treated with 2 mM thymidine (Merck Millipore, T-1895) for 18 h. After incubation, cells were washed twice with 1X PBS and released into fresh medium for 9 h (first pulse release). A second thymidine pulse was administered for an additional 18 h. At this point, cells were released from the second thymidine pulse (second pulse release) and collected at 0, 3, 4, 6, 7, 8, and 9 h for cell cycle analysis via DNA staining with EdU. To track DNA synthesis, 10 μM EdU was added at each time point for 30 min. Cells were then fixed and stained for EdU according to the manufacturer's instructions. Early, mid and late S phase cells were distinguished based on fluorescent spot patterns.[52] Cells collected at 3 h (T3) and 9 h (T9) were selected to analyze early and late S phase cells, respectively, using the DNA fiber assay. The DNA fiber assay was performed according to the protocol described in,[76] with minor modifications. Briefly, 10^5 HeLa cells we seeded and synchronized in S phase as described above. Half an hour before T3 and T9 time points, IdU thymidine analog was added at a final concentration of 25 μM for 30 min. At the end (T3 and T9 time points), cells were washed with 1X PBS and incubated for an additional 30 min with 10 μM PDS and 250 μM CldU thymidine analog. To evaluate the effect of RNase H1 overexpression and transcription inhibition on PDS-induced replication fork slowing, cells were transfected with pcDNA3-RNaseH1 plasmid 24 h before the second pulse release. Alternatively, cells were treated with 100 μM DRB for 2 h before and during IdU, CldU and PDS treatment, for a total of 3 h. For the immunofluorescence staining, cells were fixed in methanol:acetic acid (3:1) and then the slides were immersed in 2.5M HCl solution for 1 h. To detect IdU and CldU, primary antibodies anti-BrdU B44 clone (Beckton Dickinson, #347580) diluted 1:25 and anti-BrdU Bu1/75 clone (Abcam, #ab6326) diluted 1:400 were used. Goat anti-mouse 568 (Thermo Fisher Scientific, #A11031) and goat anti-rat 488 (Thermo Fisher Scientific, #A48262), both diluted 1:500, were used as secondary antibodies. After immunostaining of DNA fibers, image acquisition was performed using a Nikon A1R Confocal Microscope (Eclipse Ti2) at 40X magnification. DNA fibers were analyzed using ImageJ software. Fiber tracts lengths was measured and the ratio of CldU:IdU length was calculated. The obtained values for treated samples were reported as median values normalized on control samples.

Comet assay

Neutral Comet Assay has been performed with standard procedure as previously detailed in [40]. Briefly, HeLa cells were detached from cell plate and a cell suspension of 4 x 10^5 cells/ml was treated with 10 μM PDS or 10 μM CPT for 1 h. Treated cells were then combined with molten CometAssay LMAgarose (Bio-techne, #4250-050-02) and immediately pipetted into 20 well Comet slides. Next, slides were submerged in Lysis Solution (Bio-techne, #4250-010-01) for 1 h at 4°C and subsequently immersed in Neutral Electrophoresis Buffer (100 mM Tris pH 9, 300 mM Sodium Acetate) for 30 min at RT. Following incubation, comet slides were placed in an electrophoresis slide tray and subjected to 45 min electrophoresis at 21V using the Comet Assay Electrophoresis System II (Bio-techne, #4250-050-ES) at 4°C. After electrophoresis, slides were immersed in DNA precipitation Solution (1 M Ammonium Acetate in 95% ethanol solution) for 30 min at RT, followed by 70% ethanol for an additional 30 min, and finally dried at 37°C for 15 min. Dried agarose circles were stained using SYBR Gold Nucleic Acid Gel Stain (Thermo Fisher Scientific, #S11494) for 30 min at RT and washed with water. Slides were visualized using Nikon Eclipse 90i Microscope and tail moment quantification analysis was performed using ImageJ-Open Comet software.

Image analysis and representation

Fluorescent images were acquired using a Nikon Eclipse 90i fluorescence microscope and analyzed with ImageJ software, unless otherwise specified. Cells were categorized as either in S phase or no-S phase based on their positivity to EdU staining. In cases EdU and BrdU dual pulse labeling, cells were classified into four categories: early/mid S if they incorporated both thymidine analogs; late S if only EdU was incorporated; late G1 if only BrdU was incorporated; and early G1/G2M if neither EdU nor BrdU analogs were incorporated (indicating cells not replicating during the pulses). For analysis of micronuclei (MNi) or anaphase bridges, these structures were counted in each captured image. Like cells, micronuclei and bridges were classified as EdU +/− and/or $BrdU^{+/-}$ based on their staining patterns with EdU and BrdU. micronuclei or anaphase bridges data were reported as the number per 100 cells for each cell category, normalized or not with respect to the untreated control. For γH2AX analysis, the mean fluorescence intensity was measured for each cell with background subtraction. Additionally, the increase in γH2AX signal was evaluated in relation to the positivity or negativity of EdU staining. Data were plotted using GraphPad Prism version 9.0.0, and statistical analysis was conducted using the same software.

Cytofluorimetry

For FACS analysis HeLa cells were seeded at a density of 10^6 cells/well in 35 mm dishes. After 24h, cells were treated with 10 μM PDS or 10 μM CPT for 1 h and EdU labeling was performed as described in micronuclei section. Following the EdU administration, 9 μM CDK1-i (RO3306) was added to culture medium for 16 h to synchronize cells in G2 phase. Cells were collected at three time points: immediately after EdU treatment (t0), 6 h post EdU treatment (t6) and 16 h post EdU treatment (t16). Cells were then washed once with 1X PBS and fixed in 3.7% formaldehyde in 1X PBS for 15 min. After another wash with 1X PBS, cells were permeabilized by adding 1 mL of 0.2% Triton X-100 in 1X PBS for 10 min, followed by a 5-min wash in 1X PBS containing 3% BSA. Next, cells were centrifuged at 400 x *g* for 5 min at 4°C, and EdU detection was carried out by adding 100 μL of Click-iT Reaction cocktail, prepared according to datasheet instructions. After a 30-min incubation at RT, cells were washed with 1X PBS-3% BSA for 5 min, followed by a wash with 1X PBS. Finally, nuclear staining was performed using a 1 μg/mL DAPI solution at 4°C for 30 min. The FACS assay was conducted using the CytoFLEX S Flow Cytometer (Beckman Coulter), and data analysis was performed with CytExpert software.

Livecyte assay

Livecyte experiment was conducted to analyze cells undergoing mitosis after treatment with 1h PDS and Mre11 inhibitors (PFM01, PFM39) (see Figures 1 and S1) as well as after 1h PDS treatment in Pol η silenced HeLa cells (see Figures 6 and S6). For livecyte analysis in Mre11-inhibited cells, HeLa cells were seeded at a density of 5×10^4 cells/well in a 24-well culture plate. After 24 h, cells were treated with 10 μM PDS for 1 h and 50 μM PFM01 or PFM39 for 30 min before, during, and after 1h PDS treatment (total duration: 25.5 h) (see experimental scheme in Figure 1F). Following PDS treatment, cells were placed in the livecyte system (Phasefocus) for 24-h analysis. For livecyte analysis in Pol η-silenced cells, HeLa cells were seeded at a density of 8×10^5 cells/well in 60 mm dishes. 24 h after seeding, cells were treated with a scramble siRNA or two specific Pol η siRNAs (siRNA#1 and siRNA#4) for 24 h, then re-seeded at a density of 8×10^4 cells/well in a 24-well culture plate and silenced again for an additional 24 h. After 48 h of silencing, cells were treated with 10 μM PDS for 1 h and then placed in the livecyte system for 24-h analysis. All mitosis analyses were performed using Phasefocus analyze software (Analyze v3.12.2).

Protein extraction and western blotting

For PrimPol and Pol η immunoblots, whole cell protein extracts were prepared by lysing the cells in Laemmli Buffer (4% SDS, 20% glycerol, 0.125M Tris, 1X protease inhibitor cocktail). The lysates were sonicated for 20 min using Bioruptor Sonicator (Diagenode) and protein concentration was determined using the Lowry method. Subsequently, samples were incubated at 100°C for 5 min before loaded onto Bolt 4–12% Bis-Tris Plus (Thermo Fisher, #NW04120BOX). Proteins were then transferred onto nitrocellulose membrane (Thermo Fisher #88018) at 70V for 120 min and the transfer efficiency was evaluated by using No-Stain Protein Labeling Reagent (Invitrogen #A44449) according to manufacturer's protocols. For blocking, membranes were incubated for 1h at RT with 5% milk in TBS (20 mM Tris, 150 mM NaCl)-Tween 0.1% for PrimPol immunoblot and with 5% milk in TBS-Tween 0.5% for Polymerase η immunoblot. Next, membranes were incubated overnight at 4°C with primary antibodies: anti-PrimPol (kindly provided by A. Vindigni)[67] at 1:1000 and anti-Polymerase η (Pol H, B-7, sc-17770) at 1:250, both diluted in the respective blocking buffer. After three washes in TBS-Tween (0.1% or 0.5% Tween 20 as appropriate), membranes were incubated for 1h at RT with secondary antibodies: anti-Mouse (Santa Cruz Biotechnology, #sc2005) or Anti-rabbit (Abcam ref #ab205718) both at 1:1000 dilution. Following three additional washes in TBS-Tween (0.1% or 0.5% Tween 20 as appropriate) signals were detected using ECL (Thermo Fisher #32132) on a ChemiDoc imaging system (Biorad).

For anti-γH2AX and anti-pCHK2 immunoblots, nuclear cell extracts were obtained by resuspending the cells in Cell Lysis Buffer (5mM Pipes pH 8, 85mM KCl, 0.5% NP40, 1mM PMSF, 1X protease inhibitor cocktail). The cells were then centrifuged at 1700 x *g* for 10 min at 4°C, washed with Cell Lysis Buffer and centrifuged again. Pelleted nuclei were resuspended in RIPA buffer (50mM TrisHCl pH 7.5, 150mM NaCl, 0.5% Na Deoxycolate, 1% NP40, 0.1% SDS, 1X protease inhibitor cocktail) and incubated on ice for 10 min. Nuclei were sonicated for 5 min with Bioruptor Sonicator (Diagenode) and pelleted by centrifugation for 20 min. The supernatant was quantified using the Lowry method. Samples were incubated at 70°C for 10 min and Western Blot was performed as described above by using the following primary antibodies: anti-pH2AX (Phospho-Histone H2A.X, Ser139, 20E3; Cell Signaling

Technology #9718) diluted 1:700 in TBS-Tween 0.1%-milk 5% and anti-pCHK2 (Phospho-Chk2, Thr68, C13C1; Cell Signaling Technology #2197) diluted 1:500 in TBS-Tween 0.1%-BSA 5%. Immunoblot of BRCA2 and Top1 was performed as previously detailed in[20] and,[40] respectively. Protein band densities were quantified using ImageLab software version 4.1 with normalization to total protein (No-stain protein) or housekeeping proteins.

Bioinformatic analysis

DRIP-seq data were analyzed as previously reported here[20] GRO-seq files were mapped on hg19 human genome using bwa aligner (v. 0.7.17)[70] and filtered for alignment quality and duplicates using samtools (v. 1.15)[70] *sort*, *view* and Picard (v. 2.26.11) *MarkDuplicates* functions, respectively. Alignment files of DRIP-seq and GRO-seq were converted to bigwig files using deeptools (v. 3.5.1)[72] *bamCoverage* function using "RPGC" as normalization factor. Chip-seq data for pS2RNAPII and Pol η were downloaded from GEO as processed and normalized bigwig files. All means of biological replicates were computed using *bigwigCompare* deeptools function with "*–operation mean"* flag. All metaplots were produced using *computeMatrix* and *plotProfile* deeptools functions. Replicating zones were obtained from[41] supplementary materials and converted to BED files. Enrichment of DRIP bed regions over replicating zones were performed using bedtools (v. 2.30.0)[73] randomizing DRIP peaks over genic regions (GENCODE v19), as reported in.[40] Statistical analysis and plots were made using R base (v. 4.4.0) and ggplot2 (v. 3.5.1) library.

QUANTIFICATION AND STATISTICAL ANALYSIS

Statistical analysis

Statistical analyses were performed in GraphPad Prism or R using tests described in each figure legend. *p* values were provided as: $*p < 0.05$; $**p < 0.01$; $***p < 0.001$; $****p < 0.0001$.